



OPEN ACCESS

EDITED BY

Yi Chen,
Chinese Academy of Sciences (CAS), China

REVIEWED BY

Bin Su,
Chinese Academy of Sciences (CAS), China
Haijin Xu,
China University of Geosciences
Wuhan, China

*CORRESPONDENCE

Xiaoying Liao,
✉ xyliao@nwu.edu.cn

RECEIVED 05 March 2025

ACCEPTED 27 March 2025

PUBLISHED 22 April 2025

CITATION

Zhu B, Liao X, Gai Y, Liu L, Wang G, Pak SW and Yang W (2025) Petrogenesis of dark enclaves and magmatic processes in the early Paleozoic Fushui mafic complex from the Qinling Orogenic Belt, central China. *Front. Earth Sci.* 13:1588092. doi: 10.3389/feart.2025.1588092

COPYRIGHT

© 2025 Zhu, Liao, Gai, Liu, Wang, Pak and Yang. This is an open-access article distributed under the terms of the [Creative Commons Attribution License \(CC BY\)](https://creativecommons.org/licenses/by/4.0/). The use, distribution or reproduction in other forums is permitted, provided the original author(s) and the copyright owner(s) are credited and that the original publication in this journal is cited, in accordance with accepted academic practice. No use, distribution or reproduction is permitted which does not comply with these terms.

Petrogenesis of dark enclaves and magmatic processes in the early Paleozoic Fushui mafic complex from the Qinling Orogenic Belt, central China

Bokang Zhu, Xiaoying Liao*, Yongsheng Gai, Liang Liu, Ge Wang, Sang Wan Pak and Wenqiang Yang

State Key Laboratory of Continental Evolution and Early Life, Department of Geology, Northwest University, Xi'an, China

The dark mafic enclaves in igneous rocks provide valuable insights into the petrogenetic processes and help us understand the origin and evolution of magmas. The Early Paleozoic Fushui Complex (gabbro, hornblende gabbro and diorite) in the Qinling Orogenic Belt contains many dark enclaves, including hornblendite and dark gabbro. In this study, we systematically investigate these enclaves and the host rocks, aiming to explore their petrogenesis and relationship between the enclaves and the host rocks. On this basis, we further restored the continuous magmatic evolution of the Fushui Complex. Zircon U-Pb dating show the host rocks are crystallized at 484–492 Ma, and the hornblendite enclaves share relatively consistent crystallized ages around 500 Ma. However, some of the zircons in the hornblendite enclaves record a younger crystallized age of 475 Ma, suggesting a continuous magmatic process. The host rocks and dark gabbro enclaves exhibit arc-like trace-element signatures. In contrast, the hornblendite enclaves exhibit more variable, likely reflecting different degrees of magma mixing. While some hornblendite enclaves share similar geochemical characteristics with the host rocks, most are enriched in Th and U, depleted in high-field-strength elements and Sr, and show slightly enriched in light rare earth elements or flat REE distribution patterns. Compared to the host rocks, the hornblendites exhibit more depleted Sr-Nd isotope compositions. Trace element modeling indicates that both the enclaves and host rocks were originated from a metasomatized mantle, influenced by subducted oceanic and continental crust-derived melts. The hornblendite enclaves, characterized by orthocumulate texture, the earlier crystallization age (500 Ma), and the analysis of geochemistry and mineral chemistry, are interpreted as the early cumulates formed in a deep magma chamber, and the maximum crystallization temperature and pressure were 871°C and 13.7 kbar. The dark gabbro enclaves are characterized by fine-grained textures, field occurrence indicative of late-stage crystallization, and geochemical similarities with the host rock. These features suggest that they are the product of the rapid crystallization of the host magma at the edge of the magma chamber, then entrained by the rising magma. Their crystallization temperature and pressure are 852°C and 11.9 kbar. Integrating geochronological, geochemical, mineralogical data with previous studies, we identify three magmatic intrusion events and a subsequent greenschist-to

amphibolite-facies metamorphic overprint event within the Fushui Complex. This study represents the first detailed investigation of dark enclaves in the Fushui Complex and provide new insight into their petrogenesis and the magmatic evolution.

KEYWORDS

dark enclaves, Fushui mafic complex, hornblende composition, hornblenderich cumulates, multi-stage magmatic intrusion

1 Introduction

Dark mafic enclaves are primarily distributed within host magmatic rocks associated with subduction zone setting, and they can form through various petrogenetic processes, including (1) magma mixing between mafic and felsic magmas, (2) the interaction of quenched basic magma or broken basic dykes with colder host magmas (e.g., Didier, 1973; Eichelberger, 1980; Reid et al., 1983; Vernon, 1984), (3) incorporation of fragmented country rocks and mantle-derived minerals (Huang and Xue, 1990; Xu and Lin, 1991; 2003a; 2004; Chen and Zhou, 2003; Farner et al., 2018), (4) residual mineral after partial melting of the mantle source (White and Chappell, 1977), (5) early-stage cumulates (Pabst, 1928; Dodge and Kistler, 1990; Xu et al., 2003b; Donaire et al., 2005; Zhang et al., 2005), and (6) gas-driven filter pressing during rapid cooling (Xu et al., 2020). Notably, dark enclaves are most commonly found in intermediate to felsic host rocks, with relatively few occurrences in mafic rocks. Although the study of dark enclaves and their host rocks can provide crucial insight into the origin and evolution of magmatic systems, the diversity in their petrogenetic processes introduces ambiguity into the understanding of host rock petrogenesis.

Dark mafic enclave typical contain a variety of mafic minerals, including olivine, clinopyroxene and hornblende. Numerous studies have shown that hornblende can record significant information about magmatic evolution and is frequently used to infer magmatic processes (Bachmann and Dungan, 2002; Browne and Gardner, 2006; Ridolfi et al., 2008; 2010; Turner et al., 2013). Both primary hornblende and secondary hornblende, which forms through the transformation of early-crystallized olivine and clinopyroxene (Chang et al., 2021). Recent studies have demonstrated that the compositional variations of hornblende, particularly those displaying core-rim zoning, can reflect changes in melt composition, temperature, and pressure during crystallization in the magma chamber, or the subsequent melt/fluid alteration processes (e.g., Yu et al., 2015; Gong et al., 2018; Fang et al., 2019; Shan et al., 2021). From a mineralogical perspective, comparative analysis of hornblende composition provides valuable insights into the physicochemical conditions of magmatic evolution, thereby helping to trace the crystallization history of both the enclave and its host rock.

The Fushui Complex is the largest Early Paleozoic mafic intrusion exposed in the Qinling orogenic belt of central China (Dong et al., 1997). Its geochemical features display arc-like trace element compositions, enriched Sr-Nd-Hf isotopes signatures, and high zircon $\delta^{18}\text{O}$ values, indicating contributions from recycled subducted crust (Wang et al., 2014a; Zhang et al., 2015; Zheng et al., 2020). Previous studies have primarily focused on

timing of magmatism, the nature of the mantle source, and petrogenetic processes of mafic host rocks (Wang et al., 2014a; Zhang et al., 2015; Zheng et al., 2020). However, dark mafic enclaves within the complex have received relatively little attention and remain poorly constrained. Notably, both the Fushui mafic intrusions and their associated dark enclaves contain substantial amounts of hornblende, offering a unique opportunity to investigate the petrogenesis of enclaves and the magmatic evolution of the complex. In this study, we integrate geochronology, whole-rock geochemistry, and mineral chemistry to unravel the petrogenesis of the dark enclaves, their relationship with the host rocks, and the magmatic and metasomatic processes within the Fushui Complex. Alternatively, based on model calculations, we propose a new interpretation of the crustal signatures observed in the mantle source of the Fushui Complex. Our findings provide new insights into the petrogenesis of dark enclave in mafic rocks and enhance our understanding of the origin and evolution of the magmatic source of hydrous mafic intrusions in the North Qinling orogenic belt.

2 Geological setting

The Qinling-Dabie orogenic in central China, located between the South China Craton and the North China Craton, has undergone multistage tectonic evolution along two major tectonic zone (Zhang et al., 1995a; 1995b; 1996; Dong et al., 2011; Dong et al., 2021a; Liu et al., 2016). Bounded by the Shangdan Suture Zone and the Mianlue Suture Zone, the Qinling orogenic belt can be divided into the southern margin of North China Craton, the North Qinling Belt (NQB, mainly composed of the Kunming Group, Erlangping Group, Qinling Complex, and Danfeng Group) (Figure 1a), the South Qinling Belt (SQB), and the northern margin of the Yangtze Plate (Zhang et al., 1995a; 2001; Meng and Zhang, 2000; Dong and Santosh, 2016). The Shangdan suture zone separates the NQB from SQB (Figure 1a), and formed through the subduction and closure of the Shangdan Ocean. The suture zone exposes ophiolitic assemblages as well as subduction-related volcanic and sedimentary rocks (Zhang et al., 1995b; Dong et al., 2011). Dong et al. (2011) and Li et al. (2015) reviewed published geochronological data and proposed that the subduction-related volcanic rocks with N-MORB characteristics were formed at ca. 534–518 Ma within the Shangdan suture zone. The formation age of the island-arc rocks has been constrained as 507 ± 3 to 499.8 ± 4.0 Ma (Pei et al., 2005; Lu et al., 2009), indicating continued subduction of the Shangdan oceanic lithosphere at ca. 500 Ma. The Qinling Complex, a major component of the NQB, consists of gneisses, schists, amphibolites, and marble-calc-silicate rocks (You et al., 1991). The

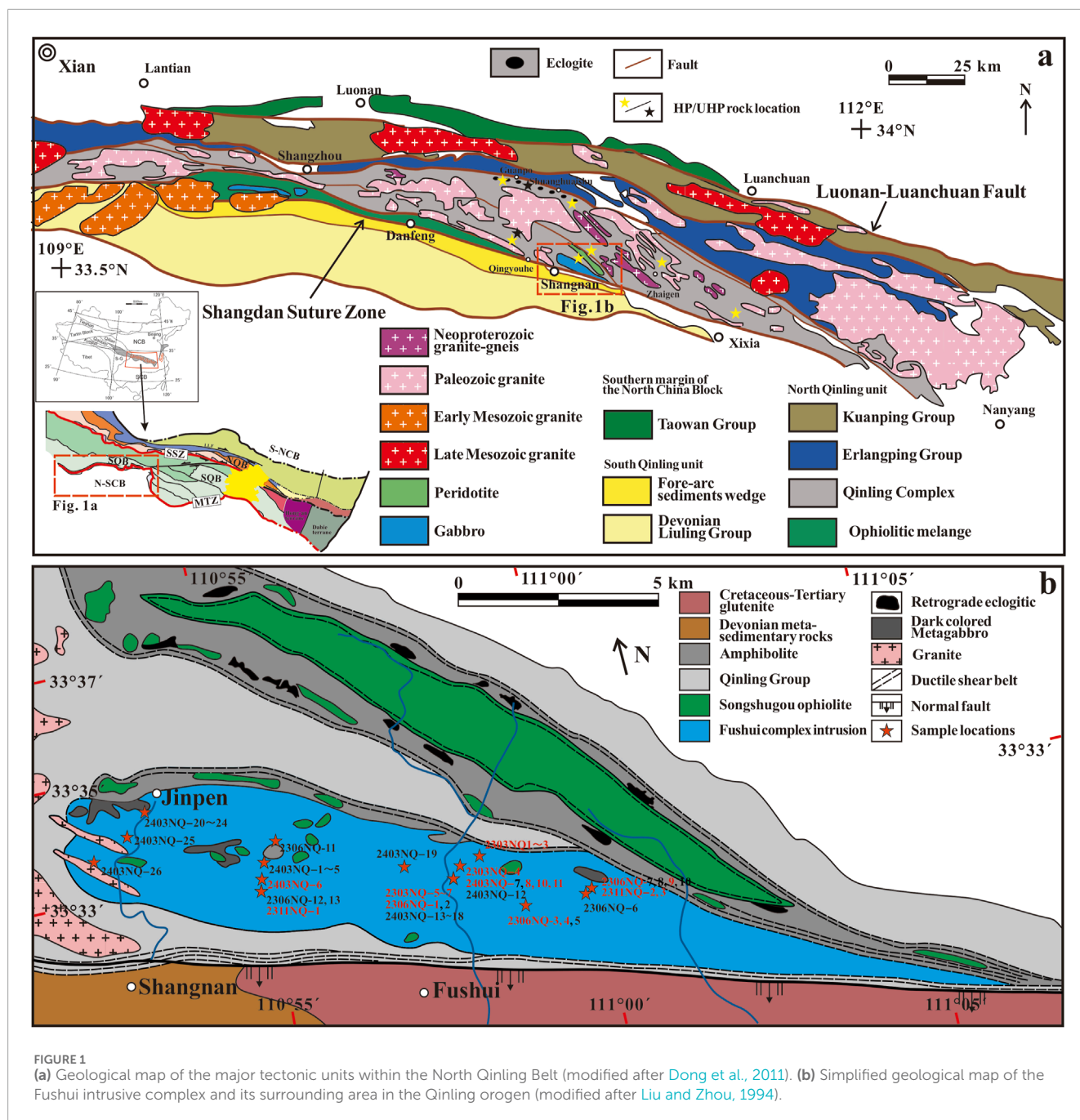


FIGURE 1 (a) Geological map of the major tectonic units within the North Qinling Belt (modified after Dong et al., 2011). (b) Simplified geological map of the Fushui intrusive complex and its surrounding area in the Qinling orogen (modified after Liu and Zhou, 1994).

high pressure-ultra high-pressure (HP-UHP) metamorphic rocks crop out in the northern, central, and southern Qinling Complex. The discovery of microdiamond and coesite inclusions from gneiss, eclogites and amphibolites (Yang et al., 2003; Wang et al., 2014b; Gong et al., 2016) confirm UHP metamorphism in the NQB. These HP-UHP rocks were interpreted as the products of deep continental subduction with metamorphic ages ranging from ca. 500–490 Ma (Yang et al., 2003; Wang et al., 2011; Liu et al., 2013; 2016; Chen et al., 2015; Liao et al., 2016). Two separate uplift events are thought to have caused the two-stage retrograde metamorphism at ca. 470–450 Ma and ca. 420 Ma (Liu et al., 2013; Chen et al., 2015; Liao et al., 2016; Hu et al., 2020).

The Fushui Complex is located to the north of the Shangdan suture zone and to the south of the Songshugou peridotites. It is the largest mafic pluton which intrudes into the gneiss of the Qinling Complex. The Fushui complex have a rod-like shape, oriented in a NWW direction, with its long axis aligned with the regional tectonic trend (Figure 1b). Early studies suggest that the Fushui Complex mainly consists of light-colored metagabbro composed of plagioclase, clinopyroxene and biotite, along with brecciated and agglomerated peridotite, dark colored metagabbro and pyroxenite in varying sizes. Additionally, the complex also includes later-formed monzonite, syenite and granite, and numerous light-colored veins (Dong et al., 1997; Chen et al., 2004;

Zhang et al., 2015). Previous studies have extensively investigated the formation age of Fushui Complex. Su et al. (2004) reported a SHRIMP zircon U-Pb age at ca. 490 Ma, while Li et al. (2006) obtained SHRIMP/TIMS zircon/baddeleyite U-Pb ages at ca. 501 and 480 Ma. Zhang et al. (2015) reported SIMS zircon U-Pb ages at ca. 497, 480–490 and 475 Ma, suggesting Fushui Complex may have experienced multi-stage, pulsed magma intrusions. The earliest stage of magmatic activity occurred ca. 500 Ma, with the main magmatic events concentrated between 480 and 490 Ma, and the latest magmatic activity around 475 Ma (Zhang et al., 2015). In addition, Wang et al. (2014a) and Zheng et al. (2020) reported SIMS/LA-ICPMS zircon U-Pb ages of 484–490 Ma, further constraining the formation age of the complex. Geochemical studies suggest that Fushui Complex exhibits arc-like characteristics, with its source derived from an enriched lithospheric mantle metasomatized by melts from ancient continental sediments and AOC (Zhang et al., 2015; Wang et al., 2014a; Zheng et al., 2020). While most studies agree on the nature of the source of the Fushui Complex, there are still different interpretations regarding its formation process. Wang et al. (2014a) proposed that the Fushui Complex formed during the northward subduction of the Paleo-Tethys Ocean beneath the North Qinling micro-continent, with partial melting of metasomatized mantle peridotite. Zhang et al. (2015) argued that Fushui Complex represents a suite of co-subducted mantle-derived magmatic activities that occurred simultaneously with UHP metamorphism. Zheng et al. (2020) suggested that the Fushui Complex formed from partial melting of the lithospheric mantle during the continental crust exhumation stage, noting that its intrusion age slightly postdates the UHP metamorphism of the NQB. Recently, Hao et al. (2022) based on the Mg-Ba-Sr-Nd isotopic data, proposed a mélange origin of Fushui Complex.

3 Field occurrences and sample descriptions

Field observations revealed that the Fushui mafic intrusive complex is primarily composed of hornblende gabbro, gabbro and diorite, with minor amounts of syenite, monzonite, and granitic dikes. Affected by the later fault zone, the internal structural deformation of the complex is very complex, and the edge has a gneissic structure and mylonitization (Figures 2i, j). Dark enclaves are common and widespread throughout the intrusion, from its core to margins. These dark enclaves include hornblende and dark gabbro. The hornblende enclaves exhibit a fine to medium-grained microgranular texture and display diverse shapes, ranging from ellipsoidal or lenticular to elongated forms, with long axes ranging from several centimeters to meters (Figures 2a–g). Most of dark gabbro enclaves are elongated strips, while a few are irregular ovals. The dark gabbro enclaves show magmatic flow structures, with the long axis aligned with the mineral orientation of the host rocks (Figure 2g). Additionally, country rock xenoliths are also developed in some dark gabbro enclaves (Figure 2h). None of the enclaves exhibit fine-grained condensed edges, and the contact boundaries with host rocks are generally smooth and irregular.

Samples from both the dark enclaves and host rocks were collected from the interior and margins of Fushui mafic intrusive

complex (Figure 1b). These samples were analyzed in detail for detailed geochemical and mineralogical studies. A summary of the mineral composition of the samples is provided in Table 1.

The host rocks of the Fushui Complex mainly consist of hornblende gabbro, gabbro and diorite. The hornblende gabbro develops medium-grained and inequigranular structure, which is composed approximately 20% Hbl, 50% Pl, 15% Bi, 10% Cpx, 5% Qtz, Ep, Zr, Ap, and Mag (Figures 3a, b). Pl and Hbl are the dominant minerals, occur as euhedral to subhedral grains. Relict cpx crystals enclosed within Hbl are typically embayed (Figure 3a), indicating the protolith of hornblende gabbro has undergone modification. Most Hbl grains exhibit a core-rim structure (Figures 3b, 8a, b), while Pl commonly displays polysynthetic twinning (Figures 8g, h). Euhedral to subhedral Ep crystals are present within Pl. The gabbro has a fine-grained, gabbroic texture, composed of approximately 25%–30% Cpx, 55% Pl, 8% Hbl, 8% Bi with accessory Zr (Figure 3c). Cpx and Pl are the dominant phase, both occurring as euhedral to subhedral grains. Cpx crystals commonly develop Hbl rims, though they are narrower than those in hornblende gabbro. The diorite develops medium-grained and inequigranular structure, which consists of around 25% Hbl, 55% Pl, 10% Bi, 10% Qtz, Zr, Ap, Ep, Ti, and Mag (Figure 3d). Pl and Hbl dominate and both minerals occur as subhedral to anhedral grains. Pl commonly develop polysynthetic twinning. The diorite appears to have undergone more extensive modification compared to the hornblende gabbro. Some feldspars develop sieve structure (Figure 3d), which have been transformed into Ep and Ser.

The hornblende enclave develops fine- to medium-grained and orthocumulate texture, which is dominated by Hbl (~80–100%), with ~10–15% Pl, ~1–3% Qtz, ~3% Ap + Zr + Ti + Mag. The hornblende enclave displays an orthocumulate texture, with idiomorphic Hbl crystals filled with anhedral Pl (Figure 4a). The Hbl crystals are arranged in a straight line and often form a 120° triple junction (Figure 4a). Some cumulate Hbl crystals retain clear cleavage (56°–124°). Pl and other minerals are primarily anhedral. In addition, a large number of Hbl develop core-rim (Figure 4b, 8d, e) and granoblastic structures (Figure 4c). Pl and intergranular Qtz tend to occur at the edges of the enclave.

The dark gabbro enclave develops fine-grained texture, which is composed of approximately 28% Hbl, 50% Pl, 12% Bi, 5% Qtz, 5% Cpx, along with Zr, Ap, Ti, and Mag (Figures 4d, e). The mineral assemblage and structure of the dark gabbro enclave are consistent with those of the host rocks, although the grain size is noticeably finer (Figure 4f). The linear alignment of the matrix Pl and Hbl is similar to the contact boundary between the enclave and the host rock (Figure 4f), further supporting the development of magmatic flow structures in the dark gabbro enclave.

4 Results

An integrated study of whole-rock compositions, Sr-Nd isotopes, mineral composition, and IA-MC-ICP-MS zircon U-Pb-Hf isotopes was conducted on these samples. Detailed analytical methods are presented in Supplementary Material 1.

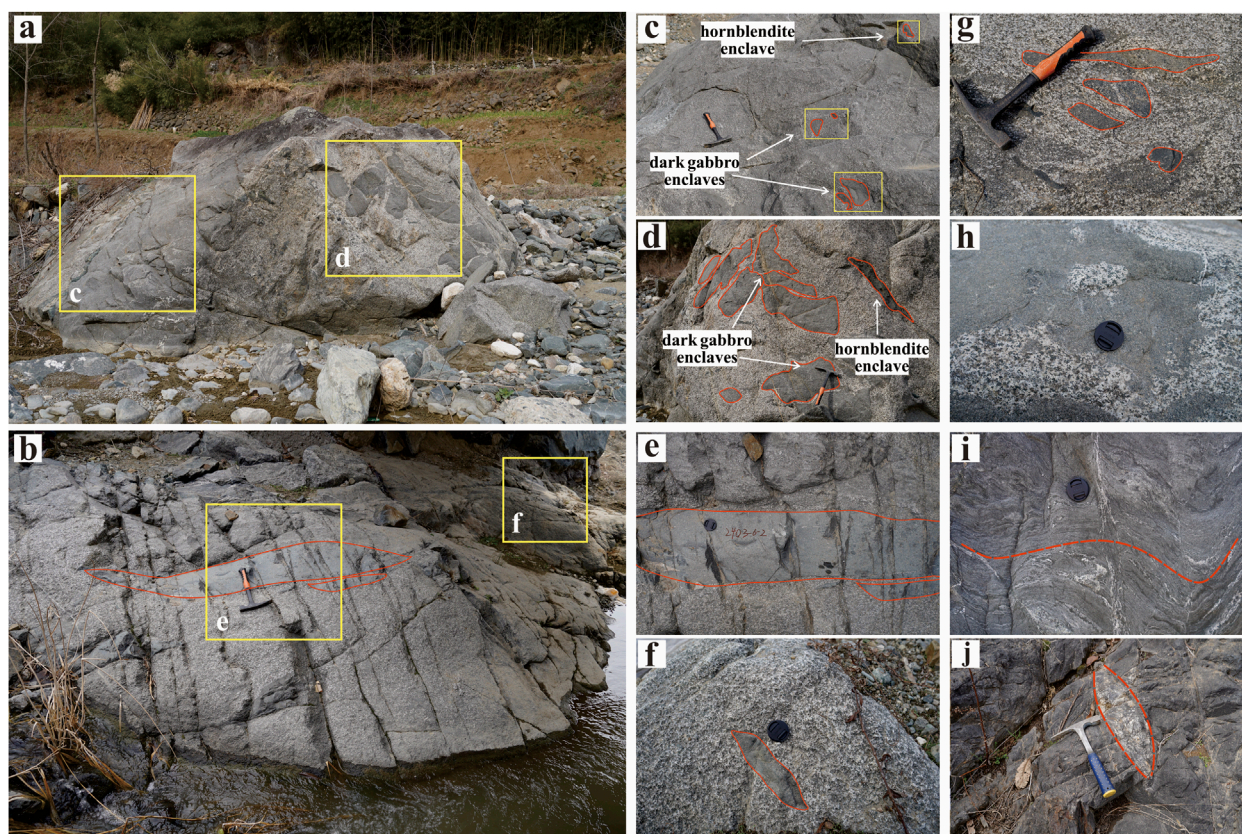


FIGURE 2

Field photographs of the dark enclaves in Fushui Complex. (a–f) Dark enclaves exhibiting various sizes and morphologies; (g) Directionally aligned dark gabbro enclaves; (h) Partial mixing between dark gabbro enclave and host diorite (i, j) Gneissic structure in the margin of the complex.

TABLE 1 Mineral modes of host rocks and enclaves in the Fushui Complex.

| Lithology | | Modes |
|------------|-------------------|--|
| Host rocks | Gabbro | 30% Cpx, 50% Pl, 10% Hbl and trace Bi and Zr |
| | Hornblende gabbro | 20% Hbl, 50% Pl, 15% Bi, 10% Cpx, and trace Qtz, Ep, Zr, Ap and Mag |
| | Diorite | 25% Hbl, 55% Pl, 10% Bi and trace Qtz, Zr, Ap, Ep, Ti, Mag and Ser |
| Enclaves | Hornblendite | 80% Hbl, 10% Pl and trace Qtz, Ap, Zr, Ti and Mag |
| | Dark gabbro | 28% Hbl, 50% Pl, 12% Bi, 5% Qtz, 5% Cpx and trace Zr, Ap, Ti and Mag |

Cpx, clinopyroxene; Hbl, hornblende; Pl, plagioclase; Mag, magnetite; Qtz, quartz; Bi, biotite; Zr, zircon; Ap, apatite; Ti, titanite; Ep, epidote; Ser, sericite.

4.1 Major and trace elements

The whole-rock major and trace element compositions are listed in [Supplementary Table S1](#).

4.1.1 The host rocks

The host rocks show variable contents of SiO₂ (43.32–56.01 wt%), Al₂O₃ (10.75–18.88 wt%), MgO (2.69–10.18 wt%), K₂O (0.7–4.73 wt%) and Na₂O (1.31–3.52 wt%). On the total alkalis vs SiO₂ (TAS) diagram, the samples plot within

the gabbro, monzogabbro and monzodiorite fields ([Figure 5a](#)). The analyzed samples exhibit high K₂O contents, predominantly falling in the shoshonitic field on the K₂O vs SiO₂ diagram ([Figure 5b](#)). In the primitive-mantle-normalized spidergrams and chondrite-normalized REE patterns ([Figures 5c, d](#)), the samples show no significant Eu anomalies, enrichment in light rare earth elements (LREE) and large-ion lithophile elements (LILE), and depletion in high-field-strength elements (HFSE) (Zr, Hf, Nb and Ta) and heavy rare earth elements (HREE). These features are characteristic of arc-type trace-element patterns.

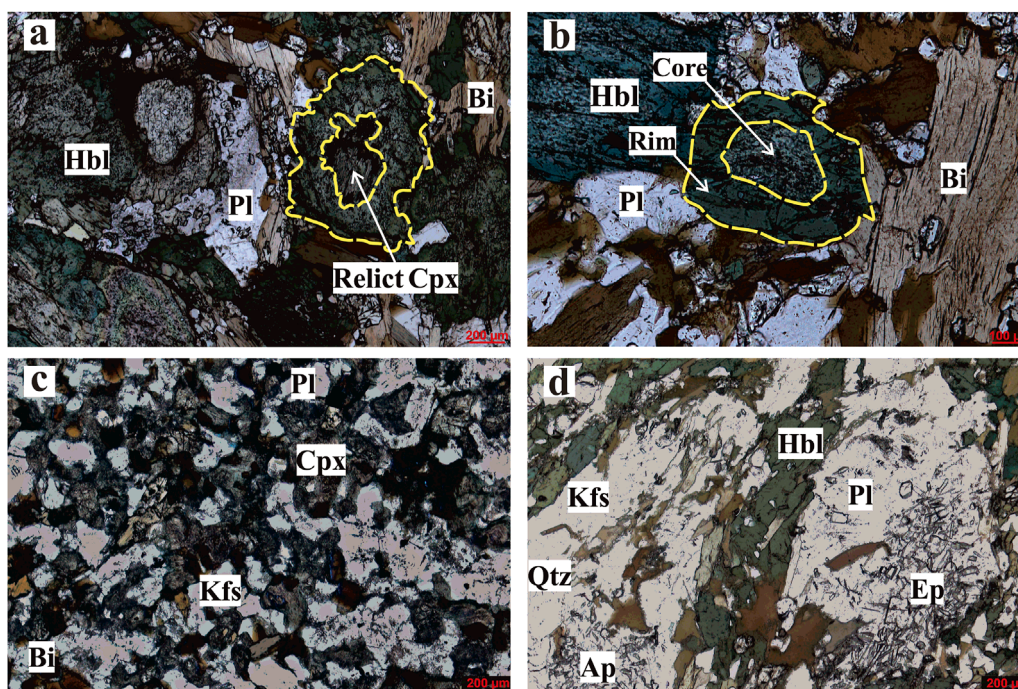


FIGURE 3 Photomicrographs of representative host rocks. **(a)** Hbl rims surround the residual Cpx in the hornblende gabbro; **(b)** Most Hbl are subhedral, with some displaying core-rim structures in the hornblende gabbro; **(c)** The fine-grained gabbro mainly consists of approximately Cpx, Pl, Hbl, and Bi; **(d)** The diorite appears to have undergone more extensive modification compared to hornblende gabbros. Numerous of Ep are present within Pl.

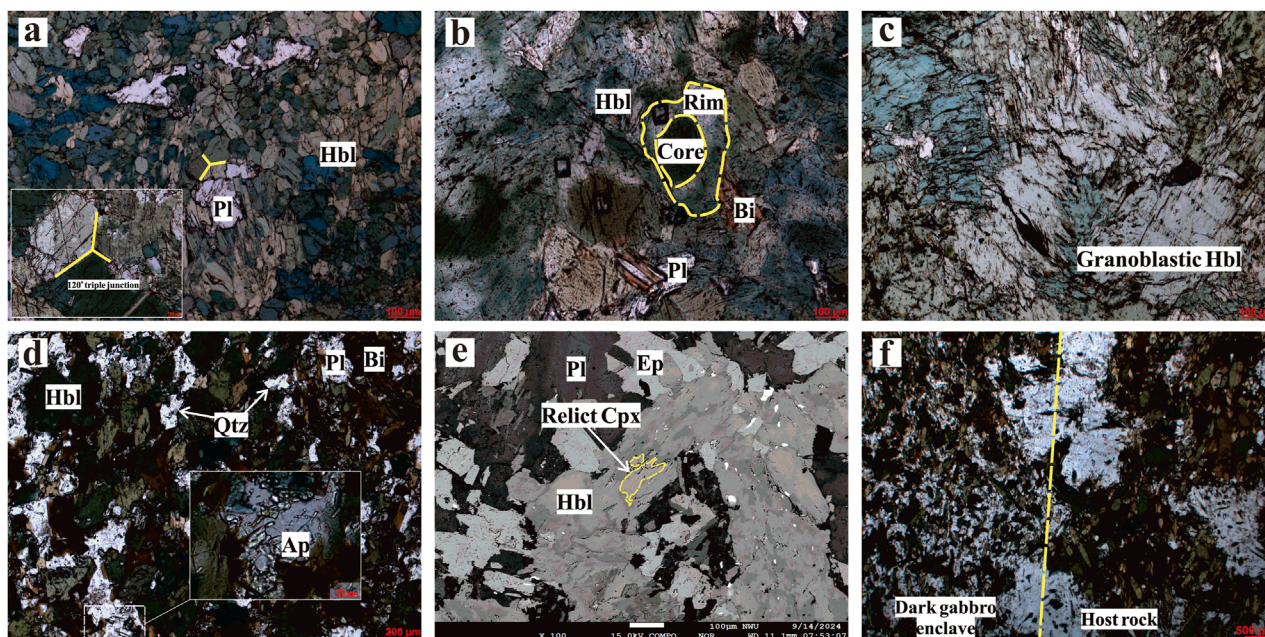
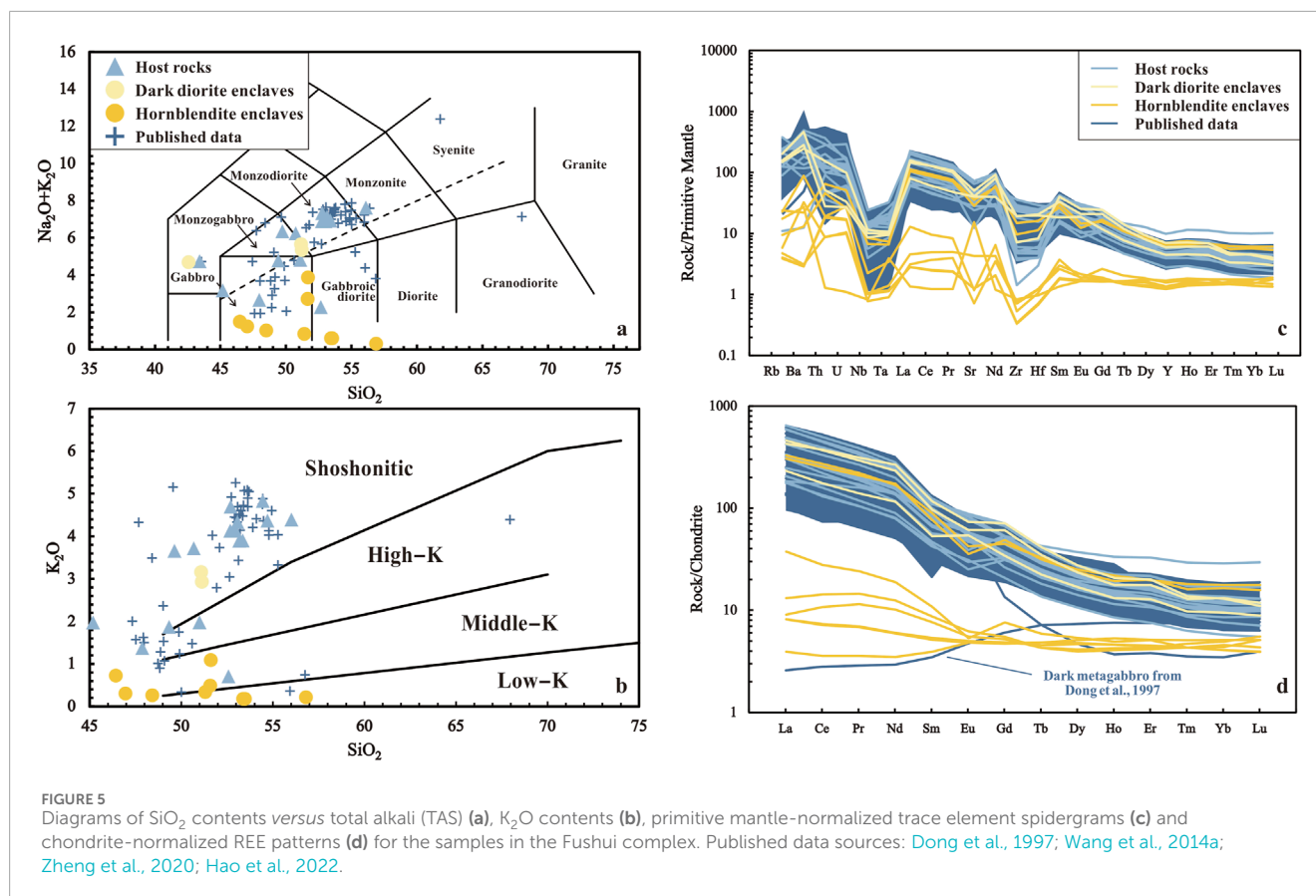


FIGURE 4 Photomicrographs of representative enclaves. **(a)** The hornblende enclave develops the granular cumulus texture; **(b)** The Hbl develops the core-rim structure; **(c)** The granoblastic Hbl in hornblende enclave; **(d)** The dark gabbro enclave is composed of Hbl, Pl, Bi, Qtz, Cpx, along with Zr, Ap, Ti, and Mag; **(e)** A very small amount of residual Cpx in the dark gabbro enclave. **(f)** The microstructures of the contact boundary between the dark gabbro enclave and host rock.



4.1.2 Hornblende enclaves

In contrast to the host rocks, the hornblende enclaves exhibit relatively low contents of SiO_2 (46.4–56.84 wt%), TiO_2 (0.02–0.73 wt%) and total alkali ($\text{K}_2\text{O} + \text{Na}_2\text{O}$) (0.36–3.91 wt%), while displaying variable high contents of MgO (6.69–17.66 wt%) and TFe_2O_3 (8.36–12.75 wt%). On the TAS diagram, the samples predominantly fall in the gabbro and gabbroic diorite fields (Figure 5a). In the K_2O vs SiO_2 diagram (Figure 5b), they mainly fall within the medium and low K_2O contents field, indicating a medium-low potassium calc-alkaline affinity. The primitive-mantle-normalized spidergrams (Figure 5c) and the chondrite-normalized REE diagram (Figure 5d) show that two samples (2306NQ-3 and 2403NQ-6) share similar trace element characteristics with the host rocks. Typical hornblende enclaves, however, are marked by a lower trace elements content, enrichment in Th and U, depletion in HFSE and Sr, and either slight enrichment in LREE or flat REE patterns. In contrast, sample 2303NQ-3 exhibits distinct trace element characteristics, including depletions in Th, U and HFSE, along with a pronounced positive Sr and Eu anomaly.

4.1.3 Dark gabbro enclaves

Similar to the host rocks, the dark gabbro enclaves have low contents of SiO_2 (42.49–51.13 wt%) and MgO (3.91–5.61 wt%), but show variable high contents of TiO_2 (0.79–1.40 wt%), TFe_2O_3 (9.37–14.07 wt%) and total alkali ($\text{K}_2\text{O} + \text{Na}_2\text{O}$) (4.75–5.72 wt%). On the TAS diagram, the samples predominantly fall within the monzodiorite fields (Figure 5a). In the K_2O vs SiO_2 diagram,

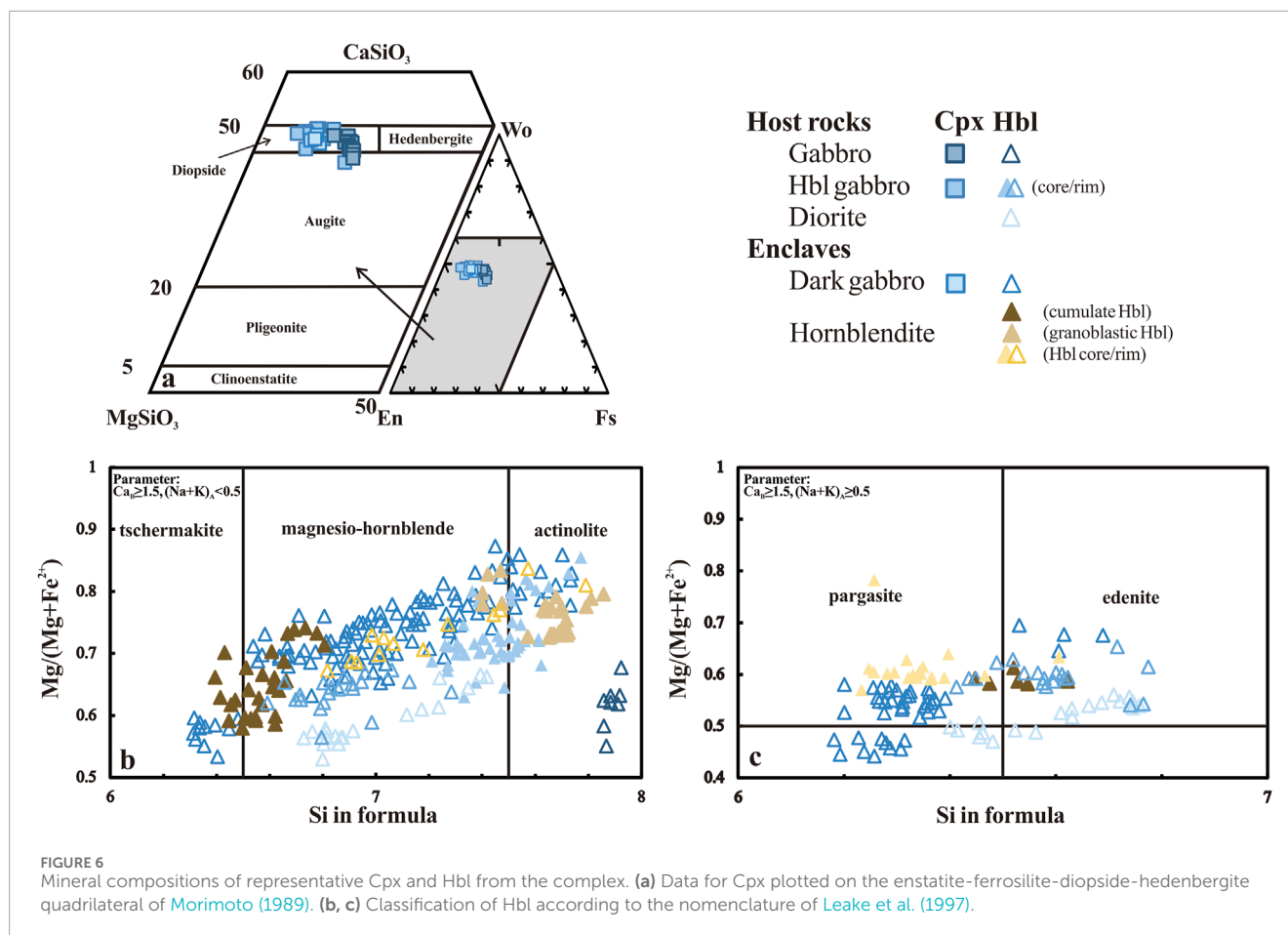
they are mainly plotted in the shoshonitic field (Figure 5b). The primitive mantle-normalized trace element characteristics and chondrite-normalized REE patterns (Figures 5c, d) further indicating that dark gabbro enclaves share similar features with the host rocks.

4.2 Mineral compositions

The major and trace elements of minerals are listed in Supplementary Table S2.

4.2.1 Clinopyroxene

Clinopyroxene appears as the main mineral phase in the gabbro, while it exists in the residual form in the hornblende gabbro and dark gabbro enclave. Grains are mainly diopside in composition (Figure 6a). Compared with the clinopyroxene in gabbro, the clinopyroxene in hornblende gabbro and dark gabbro enclave has a larger variation of SiO_2 (49.17–53.70 wt%), Al_2O_3 (0.80–4.05 wt%), higher MgO (11.95–14.96 wt%) and lower FeO_T (4.76–11.92 wt%). Because the residual clinopyroxene in the dark gabbro enclave (Figure 4e) is rare and the particle size is small, the mineral trace element analysis was not obtained. The chondrite-normalized REE distribution patterns of clinopyroxene show depletion of LREE and HREE, and obvious negative Eu anomalies (Figure 7a). However, the ΣREE of primary clinopyroxene is significantly higher than that of relict clinopyroxene (Ave. REEs is 936 and 84 ppm,



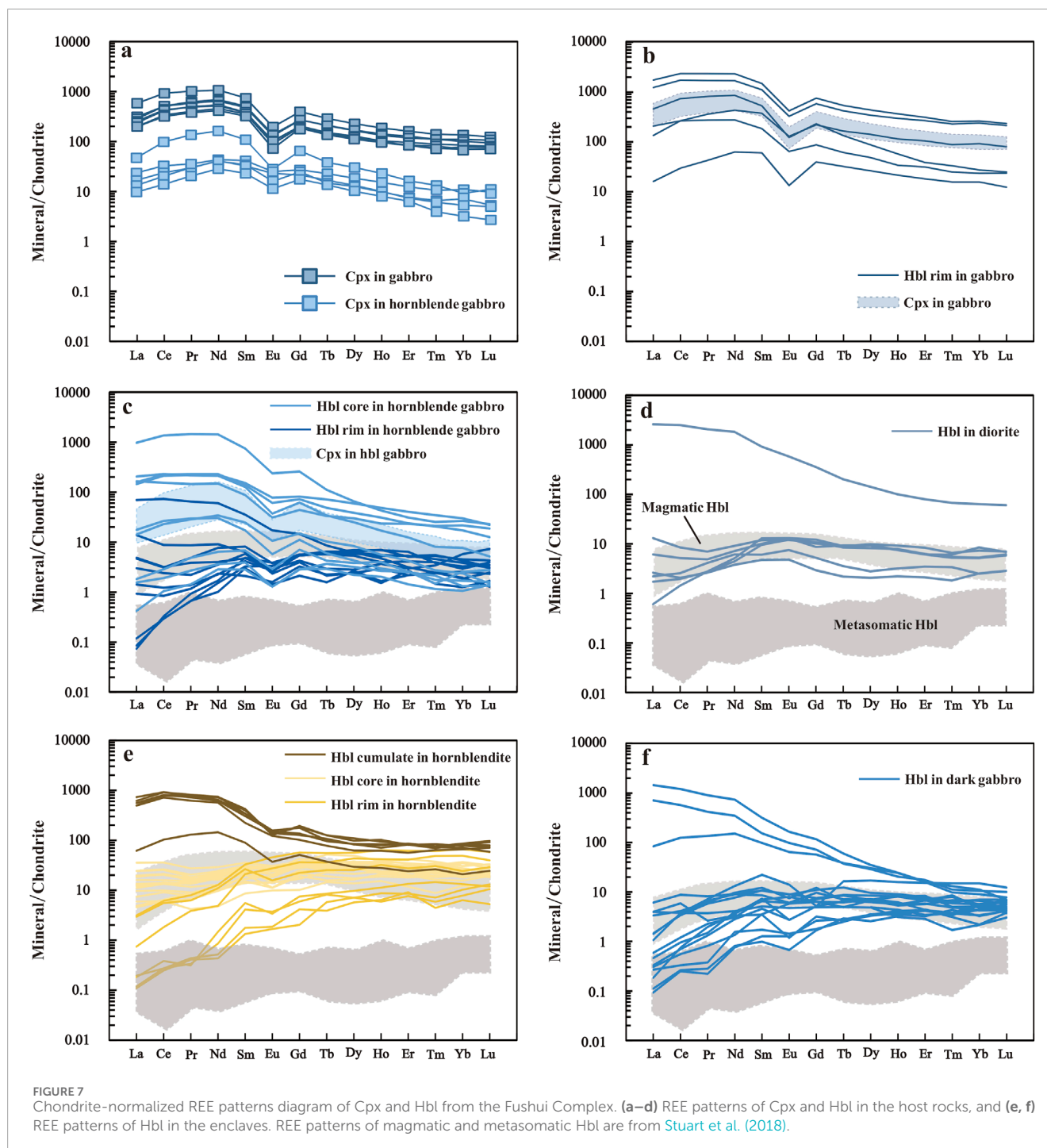
respectively), and LREE and HREE are also relatively enriched (Ave (La/Sm)_N is 0.64 and 0.47, Ave (Gd/Yb)_N is 2.66 and 4.52, respectively).

4.2.2 Hornblende

Hornblende is the predominant mafic mineral in the Fushui complex, exhibiting notable variations in the types across different samples. The hornblende occurring on the edge of clinopyroxene in the host gabbro is identified as actinolite (Figure 6b). These hornblendes display high SiO₂ contents (49.92–54.5 wt%), Mg# (55.14–71.62) values and low Al₂O₃ contents (0.55–4.22 wt%). Their REE patterns are similar to those of clinopyroxene (Figure 7b), suggesting that they are products of the clinopyroxene transformation. In the host hornblende gabbro, hornblende generally develops core-rim structure. The core predominantly consists of magnesio-hornblende and actinolite (Figure 6b), while the rim is primarily composed of magnesio-hornblende and edenite (Figures 6b, c). SiO₂ and MgO contents decrease from core to rim, corresponding with increase in Al₂O₃ and TiO₂ (Figure 8c). Regarding the REE patterns, the Hbl core displays a similar pattern to that of clinopyroxene (Figure 7c). In contrast, the REE distribution patterns of the Hbl rim can be further divided into two distinct types: one with a right-leaning, LREE-enriched or flat REE distribution curve, consistent with the magmatic hornblende (Stuart et al., 2018) and another with

LREE-depleted patterns (Figure 7c). Hornblende in the host diorite is primarily magnesio-hornblende and edenite, with significant variations in SiO₂ (41.31–53.04 wt%), Al₂O₃ (3.78–12.19 wt%) and Mg# (46.96–80.45).

The hornblende in the hornblendite enclave generally develops the cumulate, core-rim, and granoblastic structure. The cumulate Hbl is mainly Tschermakite and magnesio-hornblende, the core consists mainly of pargasite, the rim is mainly magnesio-hornblende, and the granoblastic Hbl is mainly actinolite (figures 6b, c). the cumulate Hbl has low SiO₂ content (42.94–46.41 wt%), high Al₂O₃ content (9.76–14.46 wt%) and variable Mg# (57.92–74.11), characterized by obviously enriched in LREE (Figure 7e). From the Hbl core to the rim, the contents of SiO₂ and MgO increase, while the contents of Al₂O₃ and TiO₂ decrease (Figure 8f). The Hbl core and rim also show distinct REE distribution pattern. The Hbl core has flat REE distribution curve similar to that of magmatic hornblende (Stuart et al., 2018), while the Hbl rim is characterized by LREE depletion. The granoblastic Hbl characterized by high SiO₂ (51.26–55.45 wt%) and Mg# (72.35–83.13), along with low Al₂O₃ contents (1.24–5.31 wt%), are likely of could be of late hydrothermal origins. The hornblende in the dark gabbro enclave is mainly magnesio-hornblende and pargasite (Figures 6b, c). Consistent with the hornblende in the host diorite, the hornblende in the dark gabbro enclave also has a large change in SiO₂, Al₂O₃ contents (40.03–55.72 and 2.47–13.18 wt%,



respectively) and Mg# (44.10–87.20), along with a right-leaning which is rich in LREE or flat REE distribution curve ([Figure 7f](#)).

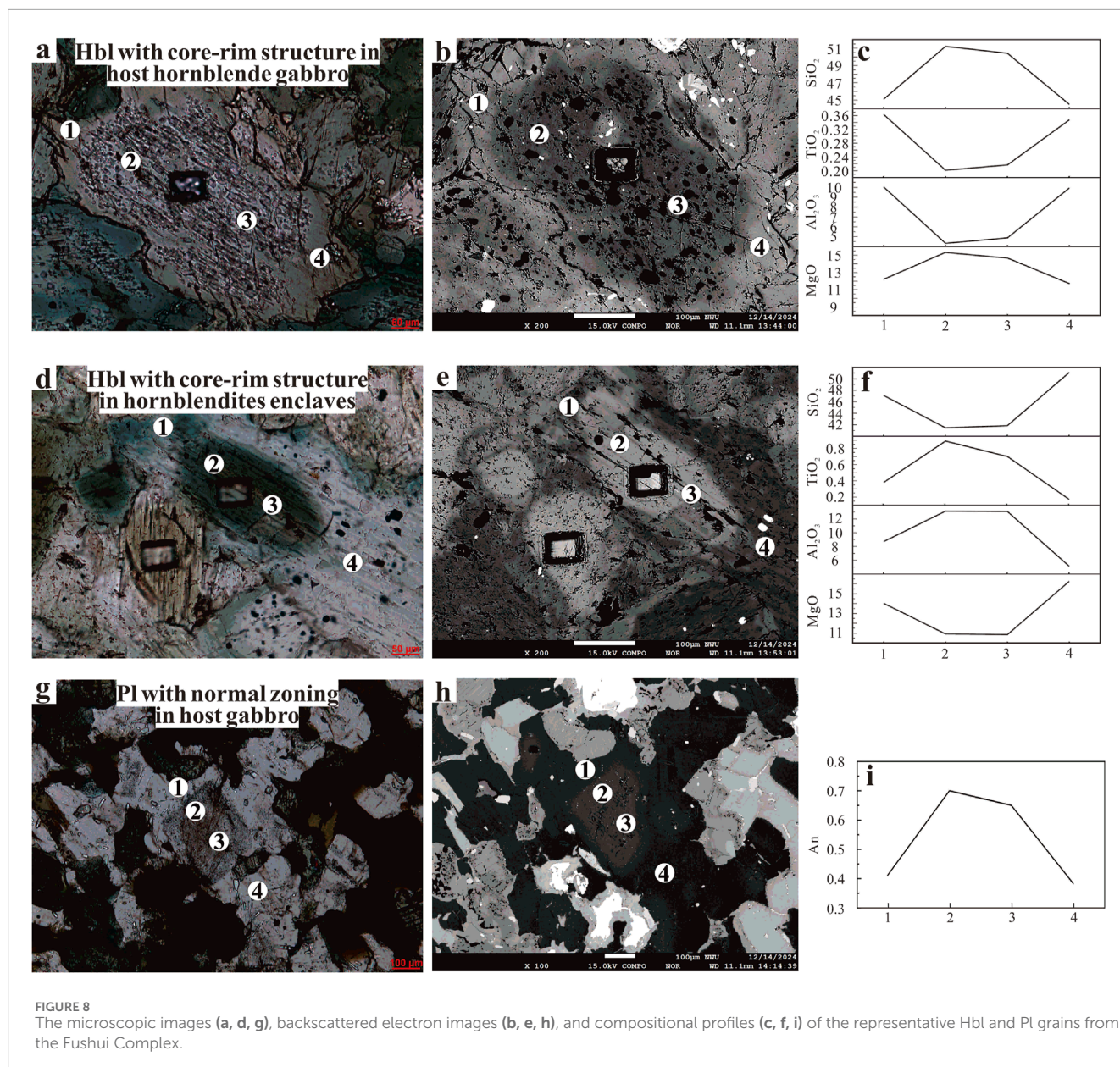
4.2.3 Plagioclase

This study analyzes plagioclase from dark gabbro enclave and the host hornblende gabbro and gabbro. Only the plagioclase in the gabbro develops zonal structure. The plagioclase in both the dark gabbro enclave and hornblende gabbro shares the similar characteristics, exhibiting highly variable An values (0.27–0.59 and 0.3–0.56, respectively). Some plagioclases in the

host gabbro show normal zonation, with decreasing An values from core to rim ([Figure 8i](#)). The An values of the core and rim range from 0.65 to 0.82 and 0.38–0.59, with average values of 0.73 and 0.47, respectively.

4.3 Pressure and temperature estimates

The chemical composition of hornblende provides valuable insights into the crystallization temperature and pressure of



magma, as well as the estimated depth of the magma chamber. In calc-alkaline magmatic systems, the Al content in hornblende is well-correlated with both the pressure and temperature during crystallization, as demonstrated in experiments studies (Blundy and Holland, 1990). As a result, several Al-in-hornblende barometry have been proposed (e.g., Hammarstrom and Zen, 1986; Hollister et al., 1987; Johnson and Rutherford, 1989; Schmidt, 1992). However, due to the lack of appropriate mineral assemblages (i.e., hornblende + biotite + plagioclase + quartz + orthoclase + titanite + ilmenite/magnetite) required for the traditional Al-in-hornblende barometry, we have chosen to apply an empirical geobarometer based on the correlation between pressure and the Al^{VI} content of igneous hornblendes (Krawczynski et al., 2012). As mentioned above, the characteristics of major and trace elements of some hornblendes in the Fushui Complex indicate their late hydrothermal origins. Therefore, the

crystallization temperature and equilibrium temperature estimates of hornblende were calculated using the thermometer models of Putirka (2016) and Liao et al. (2021), respectively. We also try to calculate the pressure and temperature of hornblende, and the water content of the melt that crystallize hornblende by using the calculation program of Ridolfi (2021). The results are presented in Table 2.

Some studies have summarized the specific cations variation of experimental hornblende from different magma compositions at different P-T conditions (e.g., Scaillet and Evans, 1999; Prouteau and Scaillet, 2003; Kiss et al., 2014; Alonso-Perez et al., 2009; Ulmer et al., 2018 and references therein). As shown in Supplementary Figure S1, most low-Al hornblendes fall into the field that were crystallized at low temperatures (700°C – 820°C) and pressures (2–3 kbar) or even lower temperature and pressure, whereas the high-Al hornblendes plot in the field that crystallized at high temperatures

TABLE 2 Pressure (P), temperature (T) and water content estimates of hornblende from host and enclave rocks in the Fushui Complex.

| Lithology | Hornblende structure | P1 (kbar) Krawczynski et al. (2012) | P2 (kbar) Ridolfi (2021) | T1 (°C) Putirka (2016) | T2 (°C) Liao et al. (2021) | T3 (°C) Ridolfi, 2021 | Water content (wt%) Ridolfi (2021) | |
|--------------|----------------------|--|-----------------------------|---------------------------|-------------------------------|--------------------------|---------------------------------------|----------|
| Host rock | Gabbro | 0.7–3.9* | 0.2–0.6 | 593–675 | 328–468* | 560–676 | 7.6–15.8 | |
| | Hornblende gabbro | 4.8–11.3* | 0.9–3.7 | 717–838* | 450–663 | 701–797 | 8.7–17.0 | |
| | | Core | 1.3–6.7* | 0.5–1.5 | 684–779 | 406–554* | 666–737 | 6.8–11.3 |
| Enclave rock | Diorite | 3.3–10.9* | 0.6–3.8 | 701–824* | 439–672 | 684–799 | 8.0–14.3 | |
| | Hornblende | Cumulate | 7.6–13.3* | 16.7–24.4 | 803–871* | 2,245–2,309 | 2,499–2,754 | 7.7–13.4 |
| | | Rim | 2.6–8.5* | 0.4–2.1 | 695–814 | 390–580* | 660–792 | 6.7–10.9 |
| Core | | 8.7–12.9* | 2.7–9.1 | 832–886* | 539–748 | 7,945–876 | 9.1–16.2 | |
| Dark gabbro | Granoblastic | 0.6–5.5* | 0.3–0.9 | 671–735 | 261–500* | 650–727 | 6.4–8.4 | |
| | — | 1.4–11.9* | 0.5–6.0 | 695–852* | 344–667 | 673–901 | 5.2–15.2 | |

*Represents the pressure and temperature estimates selected for discussion. Water content refers to the water content of the melt that crystallize hornblende.

(>800°C) and variable pressures (2–8 kbar), which provide first order constraints on the hornblende crystallization conditions. Collectively, the calculated results show the systematic changes in P-T conditions (Supplementary Figure S2). The hornblende enclaves formed under the highest pressures and temperatures (up to 13.3 kbar and 871°C), followed by the dark gabbro enclaves (up to 11.9 kbar and 852°C), with the host rocks forming at lowest pressures and temperatures (up to 11.3 kbar and 838°C) (Supplementary Figure S2). Zhang et al. (2015) suggested that the initial intrusion area may correspond to the granulite facies of the lower crust, which is consistent with the maximum pressure value (13.3 kbar) calculated in this study.

4.4 Zircon U-Pb ages

LA-MC-ICP-MS U-Pb isotope data for the zircons are present in Supplementary Table S3. Zircons are euhedral to subhedral, with sizes ranging from 80 to 220 μm and length-to-width ratios between 1:1 to 2:1. In cathodoluminescence (CL) images, the zircons exhibit broad oscillatory zoning, or weak zoning (Figure 9). Notably, several zircon grains from hornblende enclaves 2306NQ-4 show a core-rim structure, which the cores display light oscillatory zoning, while the rims are dark and unzoned, suggesting recrystallization or overgrowth during late-stage magmatic processes. All analyses reveal distinct Ce and Eu anomalies, as well as elevated high HREE concentrations (Figures 10b, d, f), indicating that these zircons are magmatic in origin, derived from mafic rock.

A total of 29 U-Pb isotopic analyses were performed on zircons from hornblende enclaves 2306NQ-4. Twenty-five of these analyses, which exhibit significant variations in Th (226–945 ppm) and U (210–2,300 ppm) contents, along with high Th/U ratios (0.80–1.32), yielded a weighted mean $^{206}\text{Pb}/^{238}\text{U}$ age of 500 ± 2 Ma (MSWD = 1.2) (Figure 10a). Notably, four analyses which exhibit significant variations in Th (388–750 ppm) and U (577–2,300 ppm) contents, along with highly variable Th/U ratios (0.17–1.03), provided a weighted mean $^{206}\text{Pb}/^{238}\text{U}$ age of 475 ± 6 Ma (MSWD = 0.3) (Figure 10a). A total of 36 U-Pb isotopic analyses were performed on zircons from diorite sample 2306NQ-2, which display highly variable Th (73–6,164 ppm) and U (111–3,630 ppm) contents, with Th/U ratios ranging from 0.17 to 1.70. 36 analyses yielded a weighted mean $^{206}\text{Pb}/^{238}\text{U}$ age of 484 ± 2 Ma (MSWD = 0.83) (Figure 10c). Additionally, 30 U-Pb isotopic analyses were performed on zircons from gabbro sample 2306NQ-9, showing wide variability in Th (82–2,618 ppm) and U (471–8,393 ppm) contents, with Th/U ratios ranging from 0.04 to 0.76. The 30 analyses yielded a weighted mean $^{206}\text{Pb}/^{238}\text{U}$ age of 492 ± 3 Ma (MSWD = 0.58) (Figure 10e).

4.5 Bulk-rock Sr-Nd and zircon Hf isotopic composition

Bulk-rock Sr-Nd isotope data of representative samples are listed in Supplementary Table S4, and zircon Hf isotope for hornblende enclave sample 2306NQ-4 are present in Supplementary Table S4.

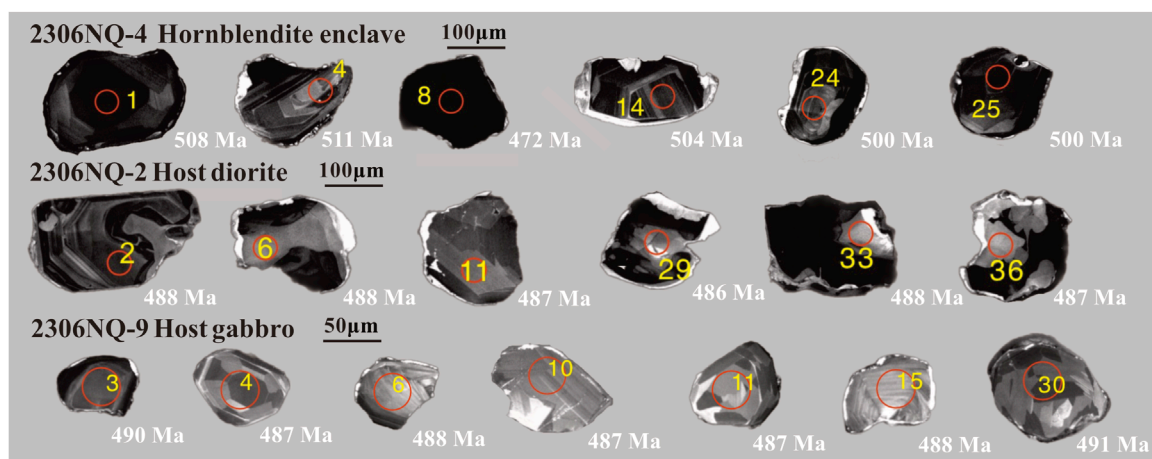


FIGURE 9
Representative zircon CL images. Circles denote the analytical spots, together with zircon U-Pb ages.

For the host gabbro, dark gabbro and hornblende enclave, the initial $^{87}\text{Sr}/^{86}\text{Sr}$ ratios and $\epsilon_{\text{Nd}}(t)$ values for whole-rock were calculated at $t = 492$ Ma, 497 Ma (Zhang et al., 2015) and 500 Ma for magma crystallization, respectively. The host gabbro and dark gabbro enclave exhibit similar Sr-Nd isotopic signatures, with high $^{87}\text{Sr}/^{86}\text{Sr}(i)$ ratios from 0.7123 to 0.7126 and 0.7135 to 0.7137, and negative $\epsilon_{\text{Nd}}(t)$ values of -5.0 to -4.6 and -5.1 to -4.5 , respectively. In contrast, the hornblende enclave shows a boarder range of Sr-Nd isotopic values, with $^{87}\text{Sr}/^{86}\text{Sr}(i)$ ratios from 0.7068 to 0.7136 and negative $\epsilon_{\text{Nd}}(t)$ values of -5.1 to -1.1 (Figure 11a). Notably, some hornblende enclaves also exhibit similar Sr-Nd isotopic signatures with the host rocks. Additionally, twenty-six zircons from the hornblende enclave yielded negative $\epsilon_{\text{Hf}}(t)$ values of -4.0 to -1.8 (Figure 11b), with two-stage Hf model ($T_{\text{DM}2}$) ages of 1,579–1717 Ma.

5 Discussion

5.1 Age of the Fushui Complex

LA-MC-ICP-MS zircon U-Pb dating of the host rocks yields weighted mean ages of 484 ± 2 Ma for the diorite (2306NQ-2), and 492 ± 3 Ma for the gabbro (2306NQ-9) (Figure 10), which consistent with previous reported ages of 484–490 Ma (Wang et al., 2014a; Zhang et al., 2015; Zheng et al., 2020). Zircon U-Pb dating of hornblende enclave reveals two age populations: 500 ± 2 and 475 ± 6 Ma (Figure 10). The dark gabbro enclave analyzed for SIMS zircon U-Pb yield weighted mean ages of 497.0 ± 18.9 and 473.0 ± 18.0 (Zhang et al., 2015). We therefore suggest that the hornblende and dark gabbro enclaves have relatively consistent zircon U-Pb ages. However, the presence of two distinct zircon age populations within the dark enclaves, along with their age differences relative to the host rocks, indicates a multi-stage crystallization history, reflecting episodic magma injection and accumulation within the magma chamber.

5.2 The nature of mantle source

5.2.1 Effects of assimilation and fractional crystallization

Crustal contamination and fractional crystallization during the emplacement can significantly modify the composition of the primary magma, but previous studies have indicated that such contamination in the Fushui Complex is minimal and can be disregarded (e.g., Wang et al., 2014a; Zheng et al., 2020; Hao et al., 2022). Accordingly, it is reasonable to conclude that the enclaves also unaffected by crustal contamination. The Fushui host mafic rocks display a wide range in SiO_2 , MgO , and $\text{Mg}\#$ values, with low Cr and Ni contents, suggesting that crystal fractionation occurred during magma ascent. Dark gabbro enclaves show similar trends, but the hornblende enclaves exhibit higher MgO , $\text{Mg}\#$, Cr and Ni contents. As shown in Figures 12a–d, MgO display a positive correlation with Ni, Cr, Sc/Y, and Ca across all samples, indicating the olivine and clinopyroxene fractional crystallization, but no significant plagioclase fractionation. Hornblende's MREE enrichment suggests differentiation between MREE and HREE, but no significant correlation between Dy/Dy^* and MgO (Figures 12e, f) indicates hornblende is not a primary fractionating phase in the host rocks.

The geochemical data suggest that its formation involved olivine and clinopyroxene crystallization. However, the fractional crystallization of these two minerals alone cannot fully explain the observed enrichment of LILE and LREE, as well as the depletion of HFSE. Furthermore, partial melting and fractional crystallization do not significantly alter isotopic compositions of mantle-derived magmas. Therefore, the geochemical composition reflects the inherited characteristics of the mantle source, providing insight into the nature of the mantle from which the magmas originated.

5.2.2 The origin of host mafic rocks

The geochemical features of the Fushui host mafic rocks exhibit high K_2O content (up to 4.73 wt%), enrichment of LILEs

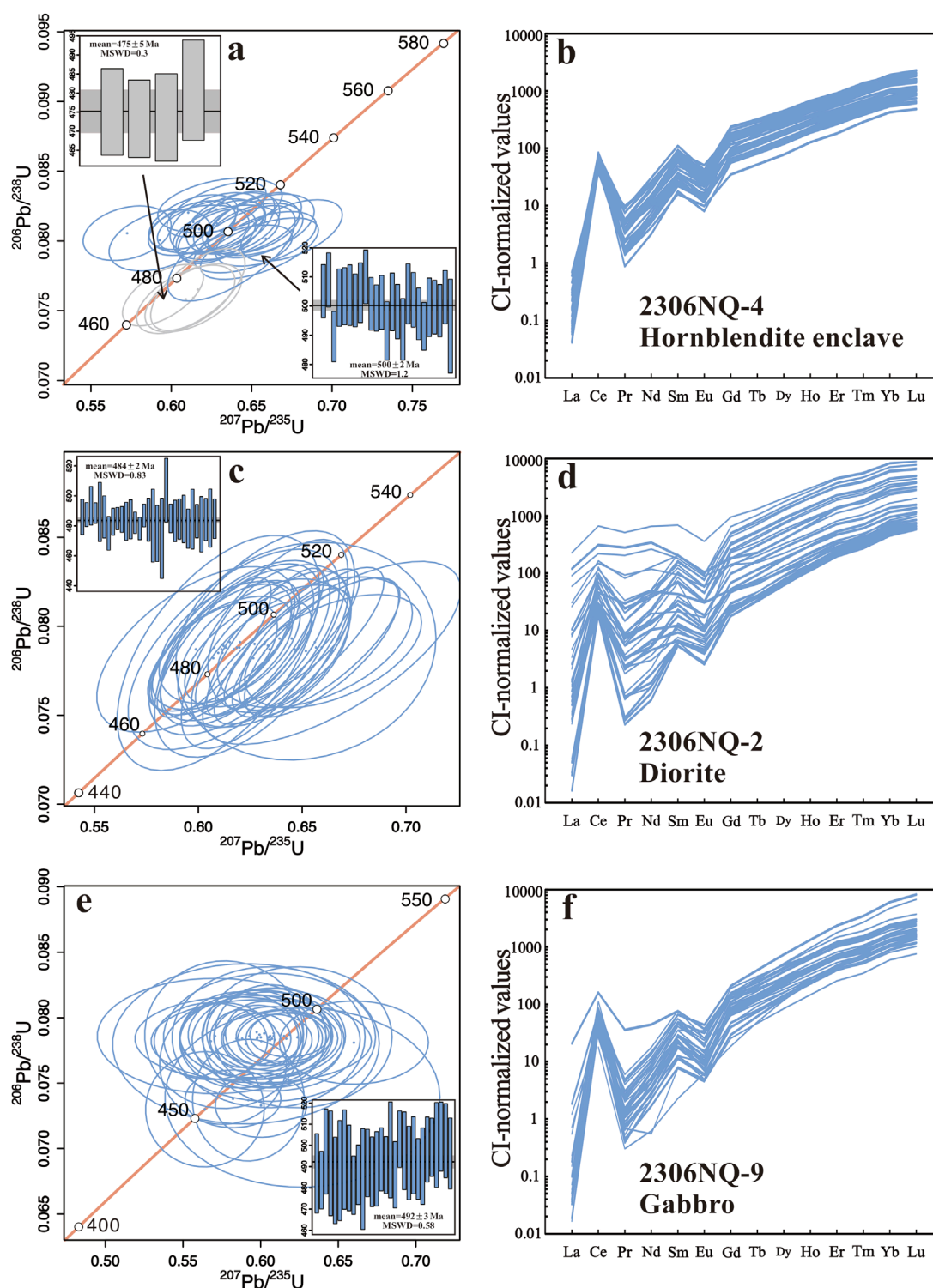
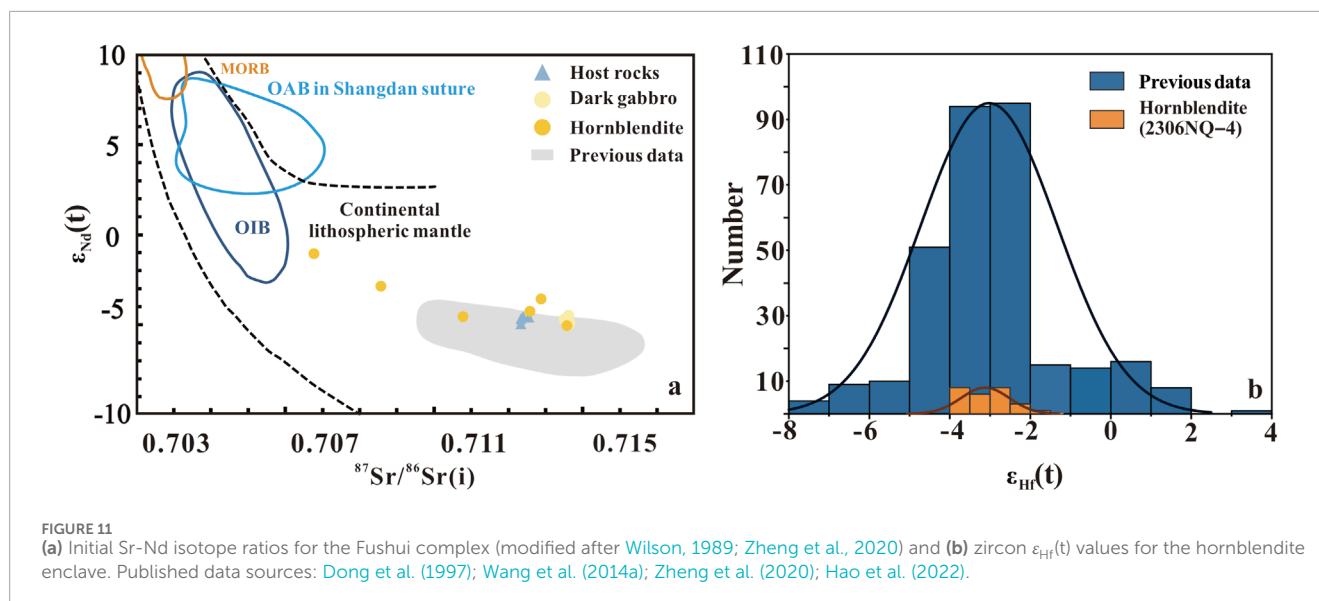


FIGURE 10 Concordia diagrams of LA-MC-ICP-MS zircon U-Pb isotope data (a, c, e) and chondrite-normalized REE patterns (b, d, f).

and LREEs, and depletion of HFSEs (Figures 5b–d). Additionally, the negative $\epsilon_{\text{Nd}}(t)$ values ($-5.0 \sim -4.6$) and high $^{87}\text{Sr}/^{86}\text{Sr}$ ratios (0.7123–0.7126) (Figure 11a) indicate that their mantle source has been modified and enriched by components with high potassium content. In contrast to the depleted mantle ($\text{K}_2\text{O} = \sim 60$ ppm;

Workman and Hart, 2005) and basaltic oceanic crust ($\text{K}_2\text{O} = \sim 0.14$ wt%; Gale et al., 2013), potassium is highly enriched in the upper crust ($\text{K}_2\text{O} = 2.80$ wt%; Rudnick and Gao, 2014). In fact, numerous studies have confirmed that recycled continental crust material plays a significant role in modifying the mantle source



of potassium-rich to ultrapotassic mafic rocks in orogenic belts (Nelson, 1992; Zhao et al., 2009; Guo et al., 2013; Tian et al., 2020). Moreover, the material sources of these recycled continental materials into the mantle are diverse. Continental materials may enter the mantle as subducted oceanic crust is accompanied by continental sediments (Nelson, 1992; Wang et al., 2016), or may be contributed by subducted continental crust (Menold et al., 2016; Hu et al., 2021).

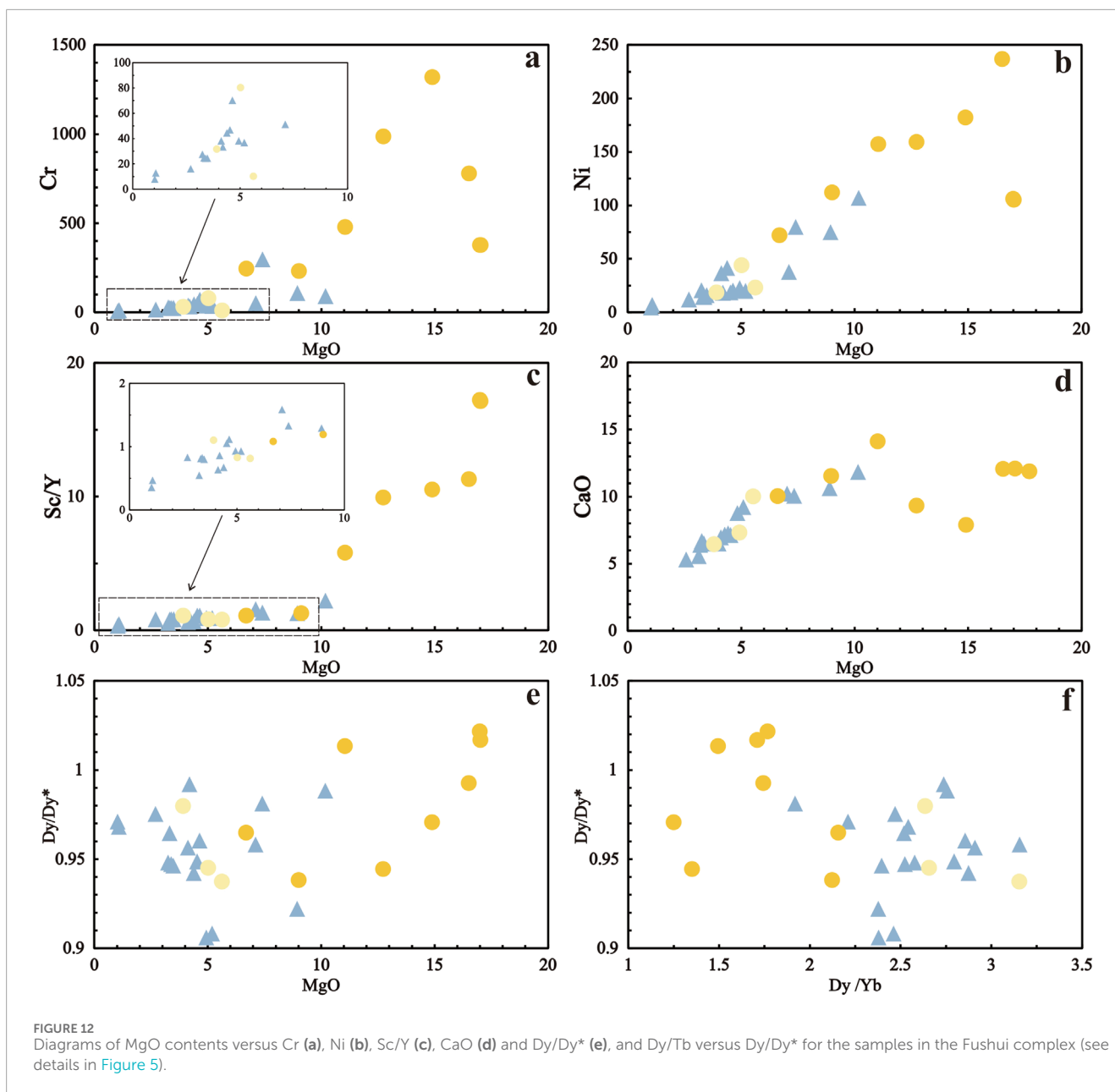
Previous geochemical study suggests that the source of the Fushui Complex derived from an enriched lithospheric mantle (Dong et al., 1997; Wang et al., 2014a; Zhang et al., 2015), metasomatized by melts and fluids from 0.5% to 2.5% ancient continental sediments and 5%–10% AOC (Zheng et al., 2020) during the subduction of Shangdan Ocean. In the present study, the spatial proximity of the Fushui Complex outcrops to the ultra-deep subducted continental material in the Songshugou area (Liu et al., 2019; Dong et al., 2021b) of the North Qinling belt, we have re-quantitatively simulated the formation of the mantle source region of hydrous metasomatic rock and the partial melting process that generates mafic magma, based on partial melting experiments of subducted continental crust. Zhang et al. (2016) found that at mantle depths within the coesite and stishovite stable fields, partial melting of subducted continental crust can generate approximately 20–30 wt% potassium-rich granitic melts and 10 wt% potassium-rich andesitic to basic (or even ultrabasic) melts, respectively. In this study, we selected pure peridotite from Songshugou in the North Qinling Belt (Su et al., 2005; Liu et al., 2007; Lee et al., 2010; Nie et al., 2017) as the mantle endmember, the mixture of subducted oceanic and continental derived melts (Zhang et al., 2016; Zang and Wang, 2022) as the crustal endmember for trace element simulation of (oceanic crust + continental crust) subduction metasomatism.

When the Songshugou peridotite (Liu et al., 2007; Lee et al., 2010; Su et al., 2005; Nie et al., 2017) is metasomatized by 10% deep subducted continental crust-derived melt (Zhang et al., 2016) or by a combination of 15% basaltic oceanic crust-derived melt (Zang and Wang, 2022) and 5% deep subducted continental crust-derived melt

(Zhang et al., 2016), the mantle metasomatites undergo low-degree (20%) partial melting, and the resulting mafic melts exhibit arc-like trace element characteristics similar to Fushui Mafic Complex (Figure 13). The results suggest that, although the proportion of ultra-deep subducted felsic continental crust-derived melt is less than 3%, it still contributes to the enrichment of incompatible elements. It is worth noting that crust-derived melts inherit the chemical properties of the initial experimental materials. At the same time, limitations in experimental petrology, such as duration and system constraints, may affect the accuracy of the results (Xu et al., 2022). Disregarding the influence of the aforementioned factors, the simulation results are generally consistent with Fushui host mafic rocks. This result indicates that the mantle source of the Fushui Complex is heterogeneous, as evidenced by the variation in bulk-rock $\epsilon_{\text{Nd}}(t)$ (−5.2~−1.2 for the hornblende enclaves and −5.0~−4.6 for the host rocks) and zircon $\epsilon_{\text{Hf}}(t)$ values (−4.0~−1.8 for the hornblende enclaves and −7.9~−3.0 for the host rocks; Wang et al., 2014a; Zhang et al., 2015; Zheng et al., 2020), likely due to the interaction of the mantle with various melt/fluid components during subduction of oceanic and continental crusts, which further complicates the compositional evolution of the mantle source.

5.3 Petrogenesis of the dark enclaves

Petrological and mineralogical observations show that the dark gabbro enclaves remain plastic upon entering into the host magma (Figure 2h), supporting the primary magma flow and emplacement. At the same time, the dark gabbro enclaves do not develop magmatic imbalance structure, which typically associated with magma mixing, such as embedded crystal structure and mineral core-rim structure. Given that both the dark gabbro enclaves and the host rocks are derived from the same mantle source, with nearly identical crystallization ages, the dark gabbro enclaves cannot be considered as refractory residue from the source area, products of magma mixing or a consolidated xenolith.



Additionally, the acicular apatite crystals and fine-grained texture within the dark gabbro enclave (Figure 4d) indicate that the parent magma has experienced quenching (Wyllie et al., 1962). Quenching is typically associated with the interaction between hot basic magma and cold acidic magma (e.g., Eichelberger, 1980; Barbarin, 2005; Vernon, 1984; Sisson et al., 1996). However, this mechanism does not explain the lacks the fine-grained quenching margins. Alternatively, some researchers have suggested that the fine-grained structure may have formed due to the contact between the parent magma and cooler surrounding rocks during its ascent and emplacement (Donaire et al., 2005; Rodríguez and Castro, 2017). As magma ascends from the deep source, it interacts with the cooler surrounding rocks, leading to rapid crystallization along the edges of the magma conduit and magma chamber. The colder regions exhibit higher pressure and crystallinity

compared to the center of the chamber, causing the melt to flow from the cooler edges toward the hotter center. This process separates the more evolved melt from fine-grained crystals, a phenomenon known as gas pressure filtration (Anderson et al., 1984; Pistone et al., 2017). During ascent, this segregation results in the formation of a more evolved melt, which develops a mineral assemblage of clinopyroxene, plagioclase, hornblende, biotite, and apatite with fine-grained structure (Figure 4d). These mineral assemblages are subsequently entrained by rising gabbroic magma, forming enclaves.

As shown in Supplementary Figure S3a, both the cumulate Hbl and Hbl core in the hornblende enclave exhibit the geochemical characteristics of mantle-derived (Supplementary Figure S3a) and magmatic hornblende (Figure 7e). Given the orthocumulate texture (Figure 4a), it is reasonable to conclude that the hornblende

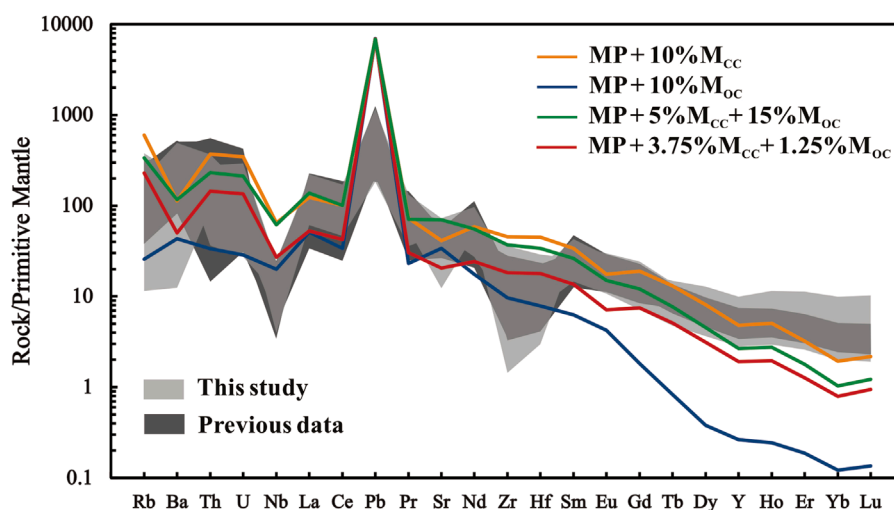


FIGURE 13

Trace element model calculation results for host rock in Fushui complex. Previous data are from Wang et al. (2014a) and Zheng et al. (2020). Abbreviations: MP, mantle peridotites; M_{cc} , continental crust-derived melt; M_{oc} , oceanic crust-derived melt.

enclave formed from cumulate processes. Experimental studies have shown that hornblende crystallization requires magma with two to three wt% H_2O (Foden and Green, 1992), and the formation of extensive hornblende cumulates likely necessitates even higher water content. The water content of the melt that crystallize hornblende in the Fushui Complex ranges from 5.24 to 16.17 wt% (Table 2), indicating that the parent magma was water-rich. High water content not reduce the melting point of mantle source, promoting partial melting and facilitating the upward migration of magma into the magma chamber (Lu et al., 2015; Rasmussen et al., 2022). As mentioned above, the Fushui Complex originated from an inhomogeneous enriched mantle metasomatized by subducted oceanic and continental crust (Figure 13). No contact metamorphism was observed between the hornblende enclaves and the host rocks (Figure 2), and the formation age of the hornblende is slightly older than that of the host rock (Figure 10). These observations suggest that a small, water-rich mantle domain underwent partial melting first, generating water-rich melts that ascended into the magma chamber. After crystallizing olivine and clinopyroxene, the water-rich melt accumulates hornblende in the deep lower crust (Figure 15a). Subsequently, the remaining metasomatized mantle underwent partial melting, with the formed melt rising into the same magma chamber, where it encased the earlier cumulate minerals, forming the hornblende enclaves.

In addition, the Hbl rim and granoblastic Hbl in the hornblende enclaves fall within the crust-mantle mixed and the crust-derived fields (Supplementary Figure S3b), which are typically attributed to magma mixing and crustal contamination (e.g., Chen et al., 2017; Chen et al., 2024; Guo et al., 2024). However, since the Fushui Complex did not undergo magma mixing and crustal contamination, implying that the hornblende in the crust-mantle mixed-derived field are mantle-derived hornblende that has undergone subsequent modification (see detailed in Section 5.4.2).

5.4 Hornblende behavior during petrogenetic processes

Zhang et al. (2015) found that the Fushui Complex recorded multi-stage magmatic intrusion events at ca. 500 Ma, 490 Ma, 480 Ma and 476 Ma, and was superimposed by metamorphism at ca. 335 Ma. Numerous studies have shown that both primary (magmatic) hornblende and secondary hornblende formed by the transformation of early crystallized olivine and clinopyroxene (Chang et al., 2021) can record important information about magmatic evolution, such as changes in melt composition, temperature and pressure during crystallization in the magma chamber, or subsequent melt/fluid alteration processes (e.g., Yu et al., 2015; Gong et al., 2018; Fang et al., 2019; Shan et al., 2021), which can be used to infer the magmatic process. Therefore, this study provides further constraints for the above process from the perspective of hornblende-related mineralogical research.

5.4.1 Multi-stage magmatic intrusion

The formation of the hornblende enclaves represents the first stage of magmatic intrusion event in the Fushui Complex, which occurred at 500 Ma.

The second magmatic event, which occurred at 484–490 Ma, is represent by the emplacement of the mafic host rocks. As shown in Table 2, the water content of the melt that crystallize hornblende in the host rock is greater than 5 wt%, indicating that the host magma is water-rich. In the process of rising into the magma chamber and wrapping the early-formed cumulate hornblende, the water-rich host magma inevitably interacts with it, which is proved by some hornblende enclaves exhibit similar geochemical characteristics and Sr-Nd isotopic signatures with the host rocks (Figures 5c, d). This reaction led to partial decomposition and recrystallization of the cumulate hornblende, forming hornblende crystals with a core-rim structure (Figure 4b), and the core-rim contact boundary is straight (Figures 8c, d). In cases where cumulate hornblende

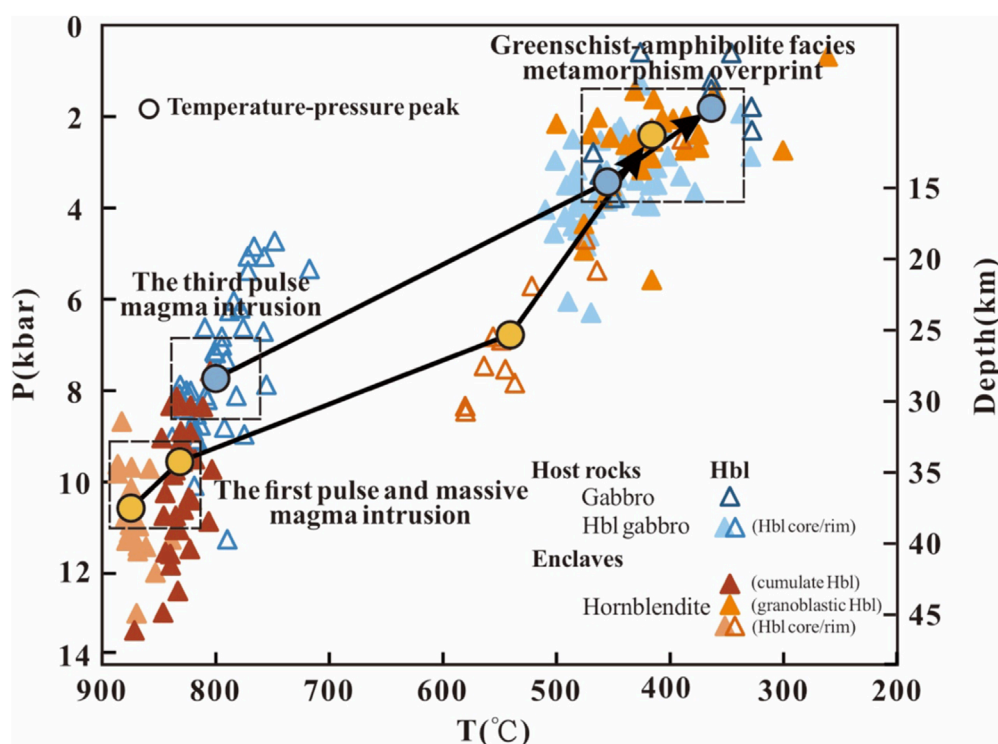


FIGURE 14
Magma emplacement process of the Fushui Complex.

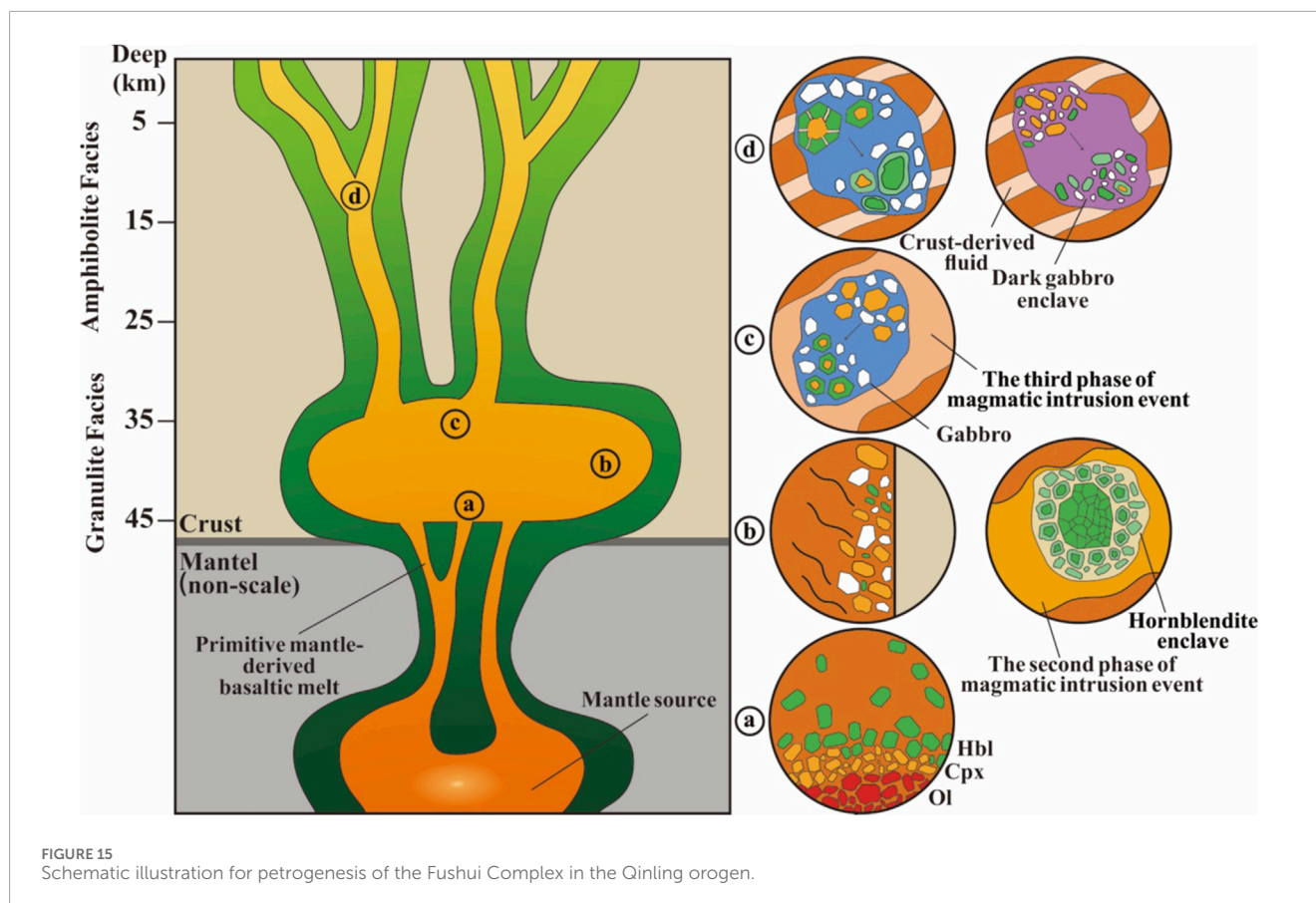
undergoes completely melting, the recrystallized hornblende will be subhedral to anhedral. The narrow interstitial space in the cumulate minerals can inhibit the migration of the melt from the edge to center of enclaves. Therefore, a textural and mineralogical transition is observed from the edge to center of hornblende enclaves, from the subhedral-anhedral crystal (Figure 4c) at the margins, to hornblende with core-rim structure (Figure 4b) and to the cumulus textures (Figure 4a) in the cores (Figure 15b). The second phase magmatic intrusion event occurs within a pressure range of 9.7–10.8 kbar and temperature of 833°C–875°C (Figure 14).

As mentioned above, the rim compositions of hornblende in the host gabbro show mineral chemical characteristics indicative of crust-mantle mixing (Supplementary Figure S3b). These chemical variations are attributed to late-stage overprinting, suggesting that unaltered hornblende rim retain a mantle-derived signature. Furthermore, the REE distribution patterns of the hornblende rim in the host hornblende gabbro is consistent with magmatic hornblende (Stuart et al., 2018) (Figure 7c). The growth of the hornblende rim represents the third stage of magmatic intrusion, which occurred at about 475 Ma, supported by zircon U-Pb ages from both hornblende enclaves in this study (Figure 10a) and dark gabbro enclaves in Zhang et al. (2015). The P-T condition for this third intrusion stage is estimated at 7.9 kbar and 800°C (Figure 14).

5.4.2 Greenschist-to amphibolite-facies metamorphism overprint

Previous studies have shown that the Fushui Complex has undergone extensive metamorphism, which has overprinted the

original features (Dong et al., 1997; Wang et al., 2014a; Zhang et al., 2015; Zheng et al., 2020). The REE distribution patterns of Hbl rim in the host gabbro and Hbl core in the host hornblende gabbro are consistent with those of clinopyroxene (Figures 7b, c), indicating that hornblende is formed by clinopyroxene through water-rock reaction. As mentioned above, the hornblendes that have the low content of TiO_2 and Al_2O_3 fall in the crust-mantle mixed-derived and the crust-derived field (Supplementary Figure S2) are not caused by magma mixing or crustal contamination, but by later transformation, which indicates that the hydrous fluid originates from the crust. And the water-rock reaction can be limited to the range of 2.0–3.5 kbar, 363°C–455°C (Figure 14). During the water-rock reaction, the crustal fluid enters through the voids of Hbl rim in the host hornblende gabbro. Due to the different degrees of reaction, some clinopyroxenes wrapped by Hbl rim are preserved (Figure 3a). However, most clinopyroxene completely reacted and formed hornblende (Hbl core) (Figure 3b) (Figure 15d). At the same time, under this unbalanced ‘semi-open system’, the hornblende formed by the reaction crystallizes a large number of minerals such as feldspar and quartz due to composition adjustment, and component diffusion occurs in the host hornblende gabbro (Figure 8b). Different from the host rocks, the dark gabbro enclaves are difficult to exist residual clinopyroxene during the reaction process because of their fine mineral particles (Figure 15d). Crust-derived fluids not only change the mineral structure and composition of clinopyroxene, but also modify the hornblende in the complex. As shown in Figure 7, it is not difficult to find that most hornblendes, especially hornblende rim in both host hornblende



gabbro and hornblende enclaves, are obviously depleted in LREE, which is likely to be the result of water-rock reaction, and also shows that the aqueous fluid is relatively depleted in LREE. At the same time, it is also due to the transformation of retrograde metamorphic fluids that hornblende in the host diorite and dark gabbro enclave exhibits a very wide T-P range (Supplementary Figures S1, S2).

(4) The magmatic emplacement was influenced by the multi-stage magmatic intrusion and greenschist-to amphibolite-facies metamorphism, which caused distinct textures and geochemical variations in the hornblende, reflecting the complex evolution of the magma.

6 Conclusion

- (1) Zircon U-Pb dating shows the hornblende enclaves crystallized around 500 Ma, while the host rocks (diorite and gabbro) crystallized at 484 Ma and 492 Ma, indicating a multi-stage magmatic process. Some hornblende enclaves contain a younger age of 475 Ma, suggesting continued magmatic activity.
- (2) The dark gabbro enclaves are geochemically similar to the host rocks, while the hornblende enclaves are not. The hornblende enclaves and host rocks with different geochemical characteristics originated from the mantle source influenced by both subducted oceanic and continental crust, representing different stages of the subduction process and mantle metasomatism.
- (3) The hornblende formed from water-rich magma that underwent partial melting in the lower crust, creating cumulates. Later, the host magma rose into the chamber, causing rapid cooling and the formation of fine-grained mineral assemblages, which led to the formation of dark gabbro and hornblende enclaves.

Data availability statement

The original contributions presented in the study are included in the article/Supplementary Material, further inquiries can be directed to the corresponding author.

Author contributions

BZ: Writing – original draft, Conceptualization, Data curation, Formal Analysis, Investigation, Methodology. XL: Conceptualization, Data curation, Formal Analysis, Funding acquisition, Investigation, Methodology, Writing – review and editing. YG: Conceptualization, Data curation, Formal Analysis, Investigation, Methodology, Writing – review and editing. LL: Conceptualization, Data curation, Formal Analysis, Funding acquisition, Investigation, Methodology, Writing – review and editing. GW: Investigation, Writing – review and editing. SP: Investigation, Writing – review and editing. WY: Data curation, Methodology, Writing – review and editing.

Funding

The author(s) declare that financial support was received for the research and/or publication of this article. This work was supported by funds from National Natural Science Foundation of China (Grant Nos. 42272059 and 42030307).

Acknowledgments

We thank Dr. Zhian Bao and Ms. Yan Zhang for zircon Hf isotope and trace elements of minerals analytical assistance, and thank Tong Li and Tuo Ma for field work.

Conflict of interest

The authors declare that the research was conducted in the absence of any commercial or financial relationships that could be construed as a potential conflict of interest.

References

- Alonso-Perez, R., Müntener, O., and Ulmer, P. (2009). Igneous garnet and amphibole fractionation in the roots of island arcs: experimental constraints on andesitic liquids. *Contributions Mineralogy Petrology* 157 (4), 541–558. doi:10.1007/s00410-008-0351-8
- Anderson, A. T., Swihart, G. H., Artioli, G., and Geiger, C. A. (1984). Segregation vesicles, gas filter-pressing, and igneous differentiation. *J. Geol.* 92 (1), 55–72. doi:10.1086/628834
- Anderson, D. L. (1989). *Theory of the earth*. Boston, MA: Blackwell Scientific, 366.
- Bachmann, O., and Dungan, M. A. (2002). Temperature-induced Al-zoning in hornblendes of the fish canyon magma, Colorado. *Am. Mineralogist* 87 (8–9), 1062–1076. doi:10.2138/am-2002-8-903
- Bao, Z., Chen, L., Zong, C., Yuan, H., Chen, K., and Dai, M. (2017). Development of pressed sulfide powder tablets for *in situ*, sulfur and lead isotope measurement using LA-MC-ICP-MS. *Int. J. Mass Spectrom.* 421, 255–262. doi:10.1016/j.ijms.2017.07.015
- Barbarin, B. (2005). Mafic magmatic enclaves and mafic rocks associated with some granitoids of the central Sierra Nevada batholith, California: nature, origin, and relations with the hosts. *Lithos* 80 (1–4), 155–177. doi:10.1016/j.lithos.2004.05.010
- Blundy, J. D., and Holland, T. B. (1990). Calcic amphibole equilibria and a new amphibole-plagioclase geothermometer. *Contributions Mineralogy Petrology* 104 (2), 208–224. doi:10.1007/bf00306444
- Browne, B., and Gardner, J. (2006). The influence of magma ascent path on the texture, mineralogy, and formation of hornblende reaction rims. *Earth Planet. Sci. Lett.* 246 (3–4), 161–176. doi:10.1016/j.epsl.2006.05.006
- Chang, J., Audétat, A., and Li, J. W. (2021). *In situ* reaction-replacement origin of hornblendites in the early cretaceous laiyuan complex, north China Craton, and implications for its tectono-magmatic evolution. *J. Petrology* 62 (5). doi:10.1093/petrology/egab030
- Chen, D. L., Ren, Y. F., Gong, X. K., Liu, L., and Gao, S. (2015). Identification and its geological significance of eclogite in Songshugou, the North qinling. *Acta Petrol. Sin.* 31 (7), 1841–1854. (in Chinese with English abstract). cnki:SUN:YSXB.0.2015-07-003.
- Chen, L. H., and Zhou, X. H. (2003). Deep-source ultramafic xenoliths in Mesozoic diorite in western Shandong and their characteristics of silicon-rich metasomatism. *Sci. China (Series D)* 33 (8), 734–744. (in Chinese with English abstract). doi:10.3969/j.issn.1674-7240.2003.08.004
- Chen, M. L., Lv, Z. Y., Ma, C. Q., Sue, G. C., He, Y. S., Wei, C. X., et al. (2024). Mineralogical characteristics of the Late Cretaceous Qianjia pluton from southwestern Hainan Island and their constraints on petrogenesis. *Geol. Bull. China* 43 (4), 503–515. (in Chinese with English abstract). doi:10.12097/gbc.2022.05.031
- Chen, Z. H., Lu, S. N., Li, H. K., Zhou, H. Y., Xiang, Z. Q., and Guo, J. J. (2004). Age of the Fushui intermediate-mafic intrusive complex in the Qinling orogen: new zircon U-Pb and whole-rock Sm and Nd isotope chronological evidence. *Geol. Bull. China* 23 (4), 322–328. (in Chinese). cnki:SUN:ZQYD.0.2004-04-003.

Generative AI statement

The author(s) declare that no Generative AI was used in the creation of this manuscript.

Publisher's note

All claims expressed in this article are solely those of the authors and do not necessarily represent those of their affiliated organizations, or those of the publisher, the editors and the reviewers. Any product that may be evaluated in this article, or claim that may be made by its manufacturer, is not guaranteed or endorsed by the publisher.

Supplementary material

The Supplementary Material for this article can be found online at: <https://www.frontiersin.org/articles/10.3389/feart.2025.1588092/full#supplementary-material>

- Chen, Z. X., Zeng, Z. G., Wang, X. Y., Yin, X. B., Chen, S., Li, X., et al. (2017). Geochemical characteristics of amphiboles in the rhyolite from the southern Okinawa Trough, and its implication for petrogenesis. *Haiyang Xuebao* 39 (12), 74–89.
- Didier, J. (1973). *Granites and their enclaves*. Elsevier Science and Technology, 393.
- Dodge, F. C. W., and Kistler, R. W. (1990). Some additional observations on inclusions in the granitic rocks of the Sierra Nevada. *J. Geophys. Res. Atmos.* 95 (B11), 17841–17848. doi:10.1029/jb095ib11p17841
- Donaire, T., Pascual, E., Pin, C., and Duthou, J. L. (2005). Microgranular enclaves as evidence of rapid cooling in granitoid rocks: the case of the Los Pedroches granodiorite, Iberian Massif, Spain. *Contributions Mineralogy Petrology* 149 (3), 247–265. doi:10.1007/s00410-005-0652-0
- Dong, J., Wei, C., and Song, S. (2021a). Deep subduction and exhumation of microcontinents in the Proto-Tethys realm: evidence from metamorphism of HP-UHT rocks in the North Qinling Orogen, central China. *Gondwana Res.* 104, 215–235. doi:10.1016/j.gr.2021.07.007
- Dong, Y., and Santosh, M. (2016). Tectonic architecture and multiple orogeny of the qinling orogenic belt, Central China. *Gondwana Res.* 29 (1), 1–40. doi:10.1016/j.gr.2015.06.009
- Dong, Y., Sun, S., Santosh, M., Zhao, J., Sun, J., He, D., et al. (2021b). Central China orogenic belt and amalgamation of east asian continents. *Gondwana Res.* 100, 131–194. doi:10.1016/j.gr.2021.03.006
- Dong, Y., Zhang, G., Neubauer, F., Liu, X., Genser, J., and Hauzenberger, C. (2011). Tectonic evolution of the Qinling orogen, China: review and synthesis. *J. Asian Earth Sci.* 41 (3), 213–237. doi:10.1016/j.jseas.2011.03.002
- Dong, Y. P., Zhou, D. W., and Zhang, G. W. (1997). GEOCHEMISTRY AND FORMATION SETTING OF FUSHUI COMPLEX, EASTERN QINLING. *Geochimica* 26 (3), 79–88. doi:10.19700/j.0379-1726.1997.03.011
- Eichelberger, J. C. (1980). Vesiculation of mafic magma during replenishment of silicic magma reservoirs. *Nature* 288, 446–450. doi:10.1038/288446a0
- Fang, L. R., Tang, D. M., Qin, K. Z., Niu, Y. J., Mao, Y. J., and Kang, Z. (2019). The indicative significance of amphibole composition to magmatic process of copper-nickel deposits in eastern Tianshan. *Acta Petrol. Sin.* 35 (7), 2061–2085. doi:10.18654/1000-0569/2019.07.08
- Farner, M. J., Lee, C. T. A., and Mikus, M. (2018). Geochemical signals of mafic-felsic mixing: case study of enclave swarms in the Bernasconi Hills pluton, California. *Geol. Soc. Am. Bull.* 130 (3–4), 649–660. doi:10.1130/b31760.1
- Foden, J. D., and Green, D. H. (1992). Possible role of amphibole in the origin of andesite: some experimental and natural evidence. *Contributions Mineralogy Petrology* 109 (4), 479–493. doi:10.1007/bf00306551
- Gale, A., Dalton, C. A., Langmuir, C. H., Su, Y., and Schilling, J.-G. (2013). The mean composition of ocean ridge basalts. *Geochem. Geophys. Geosystems* 14 (3), 489–518. doi:10.1029/2012gc004334

- Gong, L., Chen, H. Y., Xiao, B., Wang, Y. F., and Zhao, L. D. (2018). Mineral chemistry of hornblende in the Chihu-Fuxing copper district, Xinjiang, and its geological significance. *Geochimica* 47 (2), 149–168. (in Chinese with English abstract). doi:10.3969/j.issn.0379-1726.2018.02.005
- Gong, X. K., Chen, D. L., Ren, Y. F., Liu, L., Gao, S., and Yang, S. J. (2016). Identification of coesite-bearing amphibolite in the North Qinling and its geological significance. *Chin. Sci. Bull.* 61 (12), 1365–1378. doi:10.1360/N972015-01277
- Guo, J., Huang, X. L., He, P. L., and Zhong, J. W. (2024). Compositional and textural characteristics of pyroxenes and amphiboles in mesozoic high-Mg diorites from western shandong: insights into lithospheric modifications in continental interior of the North China Craton. *Geotect. Metallogenia*. doi:10.16539/j.ddgzyckx.2024.01.109
- Guo, Z., Wilson, M., Zhang, M., Cheng, Z., and Zhang, L. (2013). Post-collisional, K-rich mafic magmatism in south Tibet: constraints on Indian slab-to-wedge transport processes and plateau uplift. *Contributions Mineralogy Petrology* 165 (6), 1311–1340. doi:10.1007/s00410-013-0860-y
- Hammarstrom, J. M., and Zen, E. (1986). Aluminum in hornblende: an empirical igneous geobarometer. *71(11)*, 1297–1313. doi:10.1180/minmag.1986.050.358.28
- Hao, L. L., Nan, X. Y., Kerr, A. C., Li, S. Q., Wu, Y. B., Wang, H., et al. (2022). Mg-Ba-Sr-Nd isotopic evidence for a mélange origin of early Paleozoic arc magmatism. *Earth Planet. Sci. Lett.* 577, 117263. doi:10.1016/j.epsl.2021.117263
- Hollister, L. S., Grissom, G. C., Peters, E. K., Stowell, H. H., and Sisson, V. B. (1987). Confirmation of the empirical correlation of Al in hornblende with pressure of solidification of calc-alkaline plutons. *Am. Mineralogist* 72, 231–239.
- Hu, R.-G., Wijbrans, J. R., Brouwer, F. M., Bai, X.-J., and Qiu, H.-N. (2020). Constraints on retrograde metamorphism of UHP eclogites in North Qinling, Central China, from 40Ar/39Ar dating of amphibole and phengite. *Gondwana Res.* 87, 83–106. doi:10.1016/j.gr.2020.06.003
- Hu, Y., Teng, F.-Z., and Chauvel, C. (2021). Potassium isotopic evidence for sedimentary input to the mantle source of Lesser Antilles lavas. *Geochimica Cosmochimica Acta* 295, 98–111. doi:10.1016/j.gca.2020.12.013
- Hu, Z. C., Zhang, W., Liu, Y. S., Gao, S., Li, M., Zong, K. Q., et al. (2015). “Wave” signal-smoothing and mercury-removing device for laser ablation quadrupole and multiple collector ICPMS analysis: application to lead isotope analysis. *Anal. Chem.* 87 (2), 1152–1157. doi:10.1021/ac503749k
- Huang, F. S., and Xue, S. Z. (1990). The discovery of the Mantle-derived ultramafic xenoliths in handan xingtai intrusive complex and their mineralogical-geochemical characteristics. *Acta Petrol. Sin.* 4, 40–45. doi:10.1007/BF02919155
- Jiang, C. Y., and An, S. Y. (1983). On the chemical composition characteristics of calcareous amphibole in igneous rocks and its petrological significance. *Mineralogy Petrology* 4 (3), 1–9. doi:10.19719/j.cnki.1001-6872.1984.03.001
- Johnson, M. C., and Rutherford, M. J. (1989). Experimental calibration of the aluminum-in-hornblende geobarometer with application to Long Valley caldera (California) volcanic rocks. *Geology* 17 (9), 837–841. doi:10.1130/0091-7613(1989)017
- Kiss, B., Harangi, S., Ntaflou, T., Mason, P. R. D., and Pál-Molnár, E. (2014). Amphibole perspective to unravel pre-eruptive processes and conditions in volcanic plumbing systems beneath intermediate arc volcanoes: a case study from Ciomadul volcano (SE Carpathians). *Contributions Mineralogy Petrology* 167 (3), 986. doi:10.1007/s00410-014-0986-6
- Krawczynski, M., Grove, T. L., and Behrens, H. (2012). Amphibole stability in primitive arc magmas: effects of temperature, H₂O content, and oxygen fugacity. *Contributions Mineralogy Petrology* 164 (2), 317–339. doi:10.1007/s00410-012-0740-x
- Leake, B. E., Woolley, A. R., Arps, C. E. S., Birch, W. D., Gilbert, M. C., Grice, J. D., et al. (1997). Nomenclature of amphiboles; report of the subcommittee on amphiboles of the international mineralogical association commission on new minerals and mineral names. *Mineral. Mag.* 61 (405), 295–310. doi:10.1180/minmag.1997.061.405.13
- Lee, B., Zhu, K. M., Gong, H. J., Guo, B., Yang, T., Wang, F., et al. (2010). Genetic relationship between peridotites and chromite deposit from Songshugou area of North Qinling. *Acta Petrol. Sin.* 26 (5), 1487–1502.
- Li, H. M., Chen, Z. H., Xiang, Z. Q., Li, H. K., Lu, S. N., Zhou, H. Y., et al. (2006). Difference in U-Pb isotope ages between baddeleyite and zircon in metagabbro from the Fushui complex in the Shangnan-Xixia area, Qinling orogen. *Geol. Bull. China* 6, 653–659. doi:10.3969/j.issn.1671-2552.2006.06.001
- Li, Y., Yang, J., Dilek, Y., Zhang, J., Pei, X., Chen, S., et al. (2015). Crustal architecture of the Shangnan suture zone in the early Paleozoic Qinling orogenic belt, China: record of subduction initiation and backarc basin development. *Gondwana Res.* 27 (2), 733–744. doi:10.1016/j.gr.2014.03.006
- Liao, X., Liu, L., Wang, Y., Cao, Y., Chen, D., and Dong, Y. (2016). Multi-stage metamorphic evolution of retrograde eclogite with a granulite-facies overprint in the Zhaigen area of the North Qinling Belt, China. *Gondwana Res.* 30, 79–96. doi:10.1016/j.gr.2015.09.012
- Liao, Y., Wei, C., and Rehman, H. U. (2021). Titanium in calcium amphibole: behavior and thermometry. *Am. Mineralogist* 106 (2), 180–191. doi:10.2138/am-2020-7409
- Liu, J. F., Sun, W. D., Sun, Y., Sun, Y. L., and Liu, F. J. (2007). Geochemistry and platinum-group elements of ultramafic rocks from the Songshugou area in the eastern qinling: constraints on petrogenesis. *Geol. Rev.* 53, 1–8.
- Liu, L., Liao, X., Wang, Y., Wang, C., Santosh, M., Yang, M., et al. (2016). Early Paleozoic tectonic evolution of the North Qinling Orogenic Belt in Central China: insights on continental deep subduction and multiphase exhumation. *Earth Sci. Rev.* 159, 58–81. doi:10.1016/j.earscirev.2016.05.005
- Liu, L., Liao, X. Y., Zhang, C. L., Chen, D. L., Gong, X. K., and Kang, L. (2013). Multi-metamorphic timings of HP-UHP rocks in the North Qinling and their geological implications. *Acta Petrol. Sin.* 29 (5), 1634–1656. doi:10.3969/j.issn.1001-7143.2013.05.013
- Liu, L., Chen, D. L., Zhang, J. F., Kang, L., Wang, C., Yang, W. Q., et al. (2019). New evidence of an ultra-deep continental subduction to mantle depth (300 km) in stishovite stability field. *Earth Sci.* 44 12, 3998–4003. doi:10.3799/dqkx.2019.275
- Liu, L., and Zhou, D. W. (1994). Discovery and preliminary study of high-pressure basic granulite in Songshugou, Shangnan, East Qinling. *Chin. Sci. Bull.* 17, 1599–1601.
- Liu, Y. S., Hu, Z. C., Gao, S., Günther, D., Xu, J., Gao, C. G., et al. (2008). *In situ* analysis of major and trace elements of anhydrous minerals by LA-ICP-MS without applying an internal standard. *Chem. Geol.* 257 (1–2), 34–43. doi:10.1016/j.chemgeo.2008.08.004
- Lu, S. N., Yu, H. F., and Li, H. K. (2009). *Precambrian geology of the central orogenic belt (central-western)*. Beijing: Science Press.
- Lu, Y.-J., Loucks, R. R., Fiorentini, M. L., Yang, Z.-M., and Hou, Z.-Q. (2015). Fluid flux melting generated postcollisional high Sr/Y copper ore-forming water-rich magmas in Tibet. *Geology* 43 (7), 583–586. doi:10.1130/g36734.1
- Luo, B., Ruan, B., Zhang, H., Song, J., Xu, W., Yang, H., et al. (2024). The role of polybaric crystallization in the construction of the Gangdese continental magmatic arc, South Tibet. *Earth Planet. Sci. Lett.* 628, 118580. doi:10.1016/j.epsl.2024.118580
- Meng, Q. R., and Zhang, G. W. (2000). Geologic framework and tectonic evolution of the Qinling orogen, central China. *Tectonophysics* 323 (3–4), 183–196. doi:10.1016/s0040-1951(00)00106-2
- Menold, C. A., Grove, M., Sievers, N. E., Manning, C. E., Yin, A., Young, E. D., et al. (2016). Argon, oxygen, and boron isotopic evidence documenting 40ArE accumulation in phengite during water-rich high-pressure subduction metasomatism of continental crust. *Earth Planet. Sci. Lett.* 446, 56–67. doi:10.1016/j.epsl.2016.04.010
- Morimoto, N. (1989). Nomenclature of pyroxenes. *Mineralogical J.* 14 (5), 198–221. doi:10.2465/minerj.14.198
- Nelson, D. R. (1992). Isotopic characteristics of potassic rocks: evidence for the involvement of subducted sediments in magma genesis. *Lithos* 28 (3–6), 403–420. doi:10.1016/0024-4937(92)90016-r
- Nie, H., Yang, J., Zhou, G., Liu, C., Zheng, J., Zhang, W.-X., et al. (2017). Geochemical and Re–Os isotope constraints on the origin and age of the Songshugou peridotite massif in the Qinling orogen, central China. *Lithos* 292–293, 307–319. doi:10.1016/j.lithos.2017.09.009
- Pabst, A. (1928). *Observations on inclusions in the granitic rocks of the Sierra Nevada*, 17. University of California Publications, 325–386.
- Pei, X. Z., Li, Z. C., Ding, S. P., Li, Y., Hu, B., and Liu, H. B. (2005). Geochemical characteristics and zircon U–Pb ages of island-arc basic igneous complexes in the Tianshui area, West Qinling. *Geol. China* 32 (4), 529–540. doi:10.3969/j.issn.1000-3657.2005.04.001
- Pistone, M., Blundy, J., and Brooker, R. A. (2017). Water transfer during magma mixing events: insights into crystal mush rejuvenation and melt extraction processes. *Am. Mineralogist* 102 (4), 766–776. doi:10.2138/am-2017-5793
- Prouteau, G., and Scaillet, B. (2003). Experimental constraints on the origin of the 1991 pinatubo dacite. *J. Petrology* 44 (12), 2203–2241. doi:10.1093/petrology/egg075
- Putirka, K. (2016). Amphibole thermometers and barometers for igneous systems and some implications for eruption mechanisms of felsic magmas at arc volcanoes. *Am. Mineralogist* 101 (4), 841–858. doi:10.2138/am-2016-5506
- Rasmussen, D. J., Plank, T. A., Roman, D. C., and Zimmer, M. M. (2022). Magmatic water content controls the pre-eruptive depth of arc magmas. *Science* 375 (6585), 1169–1172. doi:10.1126/science.abm5174
- Reid, J. B., Evans, O. C., and Fates, D. G. (1983). Magma mixing in granitic rocks of the central Sierra Nevada, California. *Earth Planet. Sci. Lett.* 66, 243–261. doi:10.1016/0012-821x(83)90139-5
- Ridolfi, F. (2021). Amp-TB2: an updated model for calcic amphibole thermobarometry. *Minerals* 11 (3), 324. doi:10.3390/min11030324
- Ridolfi, F., Puerini, M., Renzulli, A., Menna, M., and Toulkeridis, T. (2008). The magmatic feeding system of El Reventador volcano (Sub-Andean zone, Ecuador) constrained by texture, mineralogy and thermobarometry of the 2002 erupted products. *J. Volcanol. Geotherm. Res.* 176 (1), 94–106. doi:10.1016/j.jvolgeores.2008.03.003
- Ridolfi, F., Renzulli, A., and Puerini, M. (2010). Stability and chemical equilibrium of amphibole in calc-alkaline magmas: an overview, new thermobarometric formulations and application to subduction-related volcanoes. *Contributions Mineralogy Petrology* 160 (1), 45–66. doi:10.1007/s00410-009-0465-7
- Rodríguez, C., and Castro, A. (2017). Silicic magma differentiation in ascent conduits. Experimental constraints. *Lithos* 272–273, 261–277. doi:10.1016/j.lithos.2016.12.017

- Rudnick, R. L., and Gao, S. (2014). "4.1-composition of the continental crust," in *Treatise on geochemistry*. 2nd ed. Amsterdam: Elsevier, 1–51.
- Scaillet, B., and Evans, B. W. (1999). The 15 June 1991 eruption of Mount Pinatubo. I. Phase equilibria and pre-eruption P-T-fO₂-fH₂O conditions of the dacite magma. *J. Petrology* 40 (3), 381–411. doi:10.1093/ptro/40.3.381
- Schmidt, M. W. (1992). Amphibole composition in tonalite as a function of pressure: an experimental calibration of the Al-in-hornblende barometer. *Contributions Mineralogy Petrology* 110 (2-3), 304–310. doi:10.1007/bf00310745
- Shan, L., Niu, Y. L., and Ma, S. L. (2021). Petrogenesis of the Neoproterozoic diorite and hornblende in the Taishan area, western Shandong: constraints on crustal evolution. *Geol. Bull. China* 40 (7), 1149–1177. (in Chinese with English abstract).
- Sisson, T. W., Grove, T. L., and Coleman, D. S. (1996). Hornblende gabbro sill complex at Onion Valley, California, and a mixing origin for the Sierra Nevada batholith. *Contributions Mineralogy Petrology* 126 (1-2), 81–108. doi:10.1007/s004100050237
- Stuart, C. A., Meek, U., Daczko, N. R., Piazzolo, S., and Huang, J.-X. (2018). Chemical signatures of melt–rock interaction in the root of a magmatic arc. *J. Petrology* 59 (2), 321–340. doi:10.1093/ptro/egy029
- Su, L., Song, S. G., Song, B., Zhou, D. W., and Hao, J. R. (2004). SHRIMP zircon U–Pb ages of garnet pyroxenite and Fushui Complex in Songshugou area and their constraints on the tectonic evolution of Qinling orogenic belt. *Chin. Sci. Bull.* 12, 1209–1211. (in Chinese). doi:10.3321/j.issn:0023-074X.2004.12.017
- Su, L., Song, S. S., and Zhou, D. W. (2005). Petrogenesis of Songshugou dunite body in the Qinling orogenic belt, Central China: constraints from geochemistry and melt inclusions. *Sci. China Ser. D Earth Sci.* 35 (1), 38–47. doi:10.1360/03yd0037
- Tian, S., Hou, Z., Mo, X., Tian, Y., Zhao, Y., Hou, K., et al. (2020). Lithium isotopic evidence for subduction of the Indian lower crust beneath southern Tibet. *Gondwana Res.* 77, 168–183. doi:10.1016/j.gr.2019.07.016
- Turner, S. J., Izbekov, P., and Langmuir, C. (2013). The magma plumbing system of Bezymianny Volcano: insights from a 54-year time series of trace element whole-rock geochemistry and amphibole compositions. *J. Volcanol. Geotherm. Res.* 263, 108–121. doi:10.1016/j.jvolgeores.2012.12.014
- Ulmer, P., Kaegi, R., and Müntener, O. (2018). Experimentally derived intermediate to silica-rich arc magmas by fractional and equilibrium crystallization at 1–0 GPa: an evaluation of phase relationships, compositions, liquid lines of descent and oxygen fugacity. *J. Petrology* 59 (1), 11–58. doi:10.1093/ptro/egy017
- Van Acherbergh, E., Ryan, C., Jackson, S., and Griffin, W. L. (2001). "Data reduction software for LA-ICP-MS." *Laser-ablation-ICPMS in the earth sciences: principles and applications*. Editor P. Sylvester (Ottawa, Canada: Mineralogical Society of Canada), 29, 239–243.
- Vernon, R. H. (1984). Microgranitoid enclaves in granites—globules of hybrid magma quenched in a plutonic environment. *Nature* 309 (5967), 438–439. doi:10.1038/309438a0
- Wang, H., Wu, Y.-B., Gao, S., Lixu, X.-C., Gong, H.-J., Li, Q.-L., et al. (2011). Eclogite origin and timings in the North Qinling terrane, and their bearing on the amalgamation of the South and North China Blocks. *J. Metamorph. Geol.* 29 (9), 1019–1031. doi:10.1111/j.1525-1314.2011.00955.x
- Wang, H., Wu, Y.-B., Gao, S., Zheng, J.-P., Liu, Q., Liu, X.-C., et al. (2014b). Deep subduction of continental crust in accretionary orogen: evidence from U–Pb dating on diamond-bearing zircons from the Qinling orogen, central China. *Lithos* 190–191, 420–429. doi:10.1016/j.lithos.2013.12.021
- Wang, H., Wu, Y. B., Li, C. R., Zhao, T. Y., Qin, Z. W., Zhu, L. Q., et al. (2014a). Recycling of sediment into the mantle source of K-rich mafic rocks: Sr–Nd–Hf–O isotopic evidence from the Fushui complex in the Qinling orogen. *Contrib. Mineral. Petrol.* 168, 1062. doi:10.1007/s00410-014-1062-y
- Wang, S.-J., Teng, F.-Z., and Scott, J. M. (2016). Tracing the origin of continental HIMU-like intraplate volcanism using magnesium isotope systematics. *Geochimica Cosmochimica Acta* 185, 78–87. doi:10.1016/j.gca.2016.01.007
- White, A. J. R., and Chappell, B. W. (1977). Ultrametamorphism and granulite genesis. *Tectonophysics* 43 (1-2), 7–22. doi:10.1016/0040-1951(77)90003-8
- Wiedenbeck, M., Hancher, J. M., Peck, W. H., Sylvester, P., Valley, J., Whitehouse, M., et al. (2004). Further characterisation of the 91500 zircon crystal. *Geostand. Geoanalytical Res.* 28, 9–39. doi:10.1111/j.1751-908x.2004.tb01041.x
- Wilson, M. (1989). "Igneous petrogenesis," in *London unwin Hyman* 325374.
- Workman, R. K., and Hart, S. R. (2005). Major and trace element composition of the depleted MORB mantle (DMM). *Earth Planet. Sci. Lett.* 231 (1-2), 53–72. doi:10.1016/j.epsl.2004.12.005
- Wyllie, P. J., Cox, K. G., and Biggar, G. M. (1962). The habit of apatite in synthetic systems and igneous rocks. *J. Petrology* 3 (2), 238–243. doi:10.1093/ptro/3.2.238
- Xu, W., Zhu, D.-C., Wang, Q., Weinberg, R. F., Wang, R., Li, S.-M., et al. (2020). Mafic microgranular enclaves formed by gas-driven filter pressing during rapid cooling: an example from the gangdese batholith in southern Tibet. *J. Petrology* 61 (11-12), 1–21. doi:10.1093/ptro/egab003
- Xu, W. L., and Lin, J. Q. (1991). The discovery and study of mantle-derived dunite inclusions in hornblende-diorite in the Handan-Xingtai area, Hebei. *Acta Geol. Sin.* 1, 33–41. doi:10.1007/BF02919155
- Xu, W. L., Ren, J., and Zhang, J. (2022). Frontiers and development strategies of experimental geoscience. *Earth Sci.* 47 (8), 2667–2678. doi:10.3799/dqkx.2022.302
- Xu, W. L., Wang, D., Gao, S., and Lin, J. Q. (2003b). The xenoliths of dunite and pyroxenite in Mesozoic Jinling diorite, western Shandong. *Chin. Sci. Bull.* 48 (8), 863–868.
- Xu, W. L., Wang, D. Y., Wang, Q. H., Gao, S., and Lin, J. Q. (2004). Metasomatism of silica-rich melts (liquids) in dunite xenoliths from western Shandong, China: implication for Mesozoic lithospheric mantle thinning. *ACTA Geol. SIN.* 78 (1), 72–80. doi:10.3321/j.issn:0001-5717.2004.01.009
- Xu, W. L., Wang, D. Y., Wang, Q. H., and Lin, J. Q. (2003a). Petrology and geochemistry of two types of mantle-derived xenoliths in Mesozoic diorite from western Shandong province. *Acta Petrol. Sin.* 19 (4), 623–636. doi:10.3969/j.issn.1000-0569.2003.04.004
- Yang, J., Xu, Z., Dobrzynetska, L., Green, H. W., Pei, X., Shi, R., et al. (2003). Discovery of metamorphic diamonds in central China: an indication of a > 4000-km-long zone of deep subduction resulting from multiple continental collisions. *Terra Nova* 15 (6), 370–379. doi:10.1046/j.1365-3121.2003.00511.x
- You, Z. D., Suo, S. T., Han, Y. J., Zhong, Z. Q., and Chen, N. S. (1991). *The metamorphic processes and tectonic analyses in the core complex of an orogenic belt: an example from the eastern Qinling mountains*. Wuhan: China University of Geosciences Press, 1–326. (in Chinese).
- Yu, M., Feng, C. Y., Liu, H. C., Li, D. W., Zhao, Y. M., Li, D. X., et al. (2015). The significance of mineralization and geochemistry of the Cl-rich amphiboles from the Galinge skarn iron deposit in Qinghai Province. *Acta Petrologica Mineralogica* 5, 721–740. doi:10.3969/j.issn.1000-6524.2015.05.010
- Yuan, H. L., Gao, S., Dai, M. N., Zong, C. L., Günther, D., Fontaine, G. H., et al. (2008). Simultaneous determination of U–Pb age, Hf isotopes and trace element compositions of zircon by excimer laser-ablation quadrupole and multiple-collector ICP-MS. *Chem. Geol.* 247, 100–118. doi:10.1016/j.chemgeo.2007.10.003
- Zang, C., and Wang, M. (2022). Effect of terrigenous sediment addition on the generation of arc silicic magma: constraints from the comparative partial melting experiment at 1.5 GPa. *Front. Earth Sci.* 10. doi:10.3389/feart.2022.851236
- Zhang, G. W., Meng, Q. R., and Lai, S. C. (1995a). The structure of Qinling orogenic belt. *Sci. China (Series B)* 25 (9), 994–1003. doi:10.1360/zb1995-25-9-994
- Zhang, G. W., Meng, Q. R., Yu, Z. P., Sun, Y., Zhou, D. W., and Guo, A. L. (1996). The orogenic process and its dynamic characteristics of the Qinling orogenic belt. *Sci. China (Series D)* 2 (1996-03-000), 193–200.
- Zhang, G. W., Zhang, B. R., Yuan, X. C., and Xiao, Q. H. (2001). *Qinling Orogenic belt and continental dynamics*. Beijing: Science Press.
- Zhang, G. W., Zhang, Z. Q., and Dong, Y. P. (1995b). Nature of main tectono-lithostratigraphic units of the Qinling orogen: implications for the tectonic evolution. *Acta Petrol. Sin.* 11 (2), 101–114.
- Zhang, H. F., Hong, Y., Zhou, D. W., Zhang, J., Dong, Y. P., and Zhang, G. W. (2015). The meta-gabbroic complex of Fushui in north Qinling orogen: a case of syn-subduction mafic magmatism. *Gondwana Res.* 28 (1), 262–275. doi:10.1016/j.gr.2014.04.010
- Zhang, J., Zhang, H. F., Ying, J. F., and Tang, Y. J. (2005). Are the peridotitic xenoliths entrained in Late Mesozoic intermediate-mafic intrusive complexes on the North China Craton the direct samples of lithospheric mantle? *Acta Petrol. Sin.* 21 (6), 1559–1568. doi:10.3321/j.issn:1000-0569.2005.06.005
- Zhang, Y., Wu, Y., Wang, C., Zhu, L., and Jin, Z. (2016). Experimental constraints on the fate of subducted upper continental crust beyond the "depth of no return." *Geochimica Cosmochimica Acta* 186, 207–225. doi:10.1016/j.gca.2016.05.002
- Zhao, Z., Mo, X., Dilek, Y., Niu, Y., DePaolo, D. J., Robinson, P., et al. (2009). Geochemical and Sr–Nd–Pb–O isotopic compositions of the post-collisional ultrapotassic magmatism in SW Tibet: petrogenesis and implications for India intra-continental subduction beneath southern Tibet. *Lithos*, 113(1-2), 190–212. doi:10.1016/j.lithos.2009.02.004
- Zheng, F., Dai, L. Q., Zhao, Z. F., Zheng, Y. F., Ma, L. T., and Fang, W. (2020). Syn-exhumation magmatism during continental collision: geochemical evidence from the early Paleozoic Fushui mafic rocks in the Qinling orogen, Central China. *Lithos* 352–353, 105318. doi:10.1016/j.lithos.2019.105318
- Zong, K. Q., Klemd, R., Yuan, Y., He, Z. Y., Guo, J. L., Shi, X. L., et al. (2017). The assembly of Rodinia: the correlation of early Neoproterozoic (ca. 900 Ma) high-grade metamorphism and continental arc formation in the southern Beishan Orogen, southern Central Asian Orogenic Belt (CAOB). *Precambrian Res.* 290, 32–48. doi:10.1016/j.precamres.2016.12.010